NASA CR-159655
FR-11662

LAMINATED TURBINE VANE DESIGN AND FABRICATION

by W. G. Hess

UNITED TECHNOLOGIES CORPORATION
PRATT & WHITNEY AIRCRAFT GROUP
GOVERNMENT PRODUCTS DIVISION

prepared for

NATIONAL AERONAUTICS AND SPACE ADMINISTRATION

NASA Lewis Research Center
Contract NAS 3-20587

1. Report No.	2. Government Accession No.	3. Recipient's Catalog No.
NASA CR-159655		

4. Title and Subtitle	5. Report Date
LAMINATED TURBINE VANE DESIGN AND FABRICATION	19 October 1979
	6. Performing Organization Code
7. Author(s)	8. Performing Organization Report No.
W. G. Hess	FR-11662
	10. Work Unit No.
9. Performing Organization Name and Address United Technologies Corporation Pratt & Whitney Aircraft Group Government Products Division West Palm Beach, Florida 33402	11. Contract or Grant No. NAS 3-20587
	13. Type of Report and Period Covered Final Report 20 December 1976 - 20 March 1979
12. Sponsoring Agency Name and Address National Aeronautics and Space Administration Contractor - Lewis Research Center Cleveland, Ohio 44135	14. Sponsoring Agency Code

15. Supplementary Notes

The airfoil design was conducted by G. P. Liang of Pratt & Whitney Aircraft and the program was sponsored by NASA Lewis Research Center under contract NAS3-20587, directed by H. J. Gladden.

16. Abstract

A turbine vane and associated endwalls were designed for advanced engine conditions supplied by NASA. The advanced vane design investigation resulted in an effectively cooled scheme that combined the cooling methods of convection and full coverage film cooling. The design incorporated the cooling benefits available through the utilization of Pratt & Whitney Aircraft's unique wafer fabrication concept. Upon completion of the design task, two vanes and associated endwalls of the final configuration were fabricated, cold flowed, and shipped to NASA for experimental evaluation in their high temperature one-vane test tunnel.

17. Key Words (Suggested by Author(s))	18. Distribution Statement
Turbine Vane and Blade Turbine Cooling Airfoil Fabrication Laminated Airfoil	Unclassified - Unlimited N79-33204#

19. Security Classif. (of this report)	20. Security Classif. (of this page)	21. No. of Pages	22. Price*
Unclassified	Unclassified	70	$3.00

* For sale by the National Technical Information Service, Springfield, Virginia 22161

CONTENTS

ILLUSTRATIONS

TABLES

I. SUMMARY

A design and fabrication effort was conducted using the Pratt & Whitney Aircraft Group (P&WA) wafer fabrication concept for an advanced engine turbine vane and associated endwalls. The construction concept involves the fabrication of airfoils from a stack of laminates (wafers) which have the desired cooling passage geometry photo-etched on the surface. The wafers are then diffusion-bonded and the final airfoil shape is machined from the bonded block to produce the finished turbine vane with integral cooling passages.

The advanced vane design combined the methods of convection cooling and selective areas of full coverage film cooling. The full coverage film cooling technique was utilized on the leading edge, pressure side, and endwall regions. It was not employed on the suction side of the vane due to the adverse aerodynamic penalties associated with film cooling in that region because of the relatively high main stream velocity.

The predicted surface temperature profile at the design point for the midspan section of the vane indicated a maximum temperature of 1059°C (1939°F). This temperature is below the design life requirement upper limit of 1079°C (1975°F) and results in oxidation/erosion life of approximately 245 hr based on the life data for the vane material – MAR-M 200 + Hf (PWA 1422). The only thermal transient condition defined was ten thermal cycles of the vane between design conditions and ambient conditions. The predicted maximum strain range was 0.32% which corresponds to a pseudo-cyclic life in excess of 10^5 cycles based on the fatigue life data for PWA 1422.

Upon completion of the design task, two vanes and associated endwalls were fabricated to the final configuration. Before shipment to NASA both vanes and associated endwalls were cold air flow calibrated to determine the cold flow characteristics. The cold flow results for the two vane airfoils indicated excellent agreement between the prediction and the experimental data. The flow characteristics of the endwalls were also determined for both vanes; however, the experimental data indicated a severe underflowing condition when compared to the prediction. A portion of this is attributed to a number of endwall passages that did not open up during final machining operations. It is recommended that the endwalls be flow-checked again before hot cascade tests are conducted to define flow conditions required for the hot tests.

II. INTRODUCTION

Turbine inlet temperatures and pressures for advanced gas turbine engines have progressed to levels where convection cooling schemes are inadequate. To maintain reasonable wall temperatures in advanced turbines, more sophisticated cooling schemes are required. A method of approach, which is relatively efficient, is full-coverage film cooling combined with an effective convection cooling scheme. One method to accomplish this is to perforate a cast hollow airfoil with hundreds of small holes. This method is expensive and is hindered by fabrication and structural limitations on the minimum size and shape of the holes. This limits the effectiveness of these cooling schemes. A potential solution to this problem is to construct the airfoil of horizontally or radially stacked wafers with the desired cooling passage geometry photo-etched on the surface. This affords more flexibility in passage size and shape which can result in improved cooling effectiveness.

The vane designed and constructed for this program utilized this wafer fabrication concept. This concept involves the fabrication of airfoils from a stack of wafers. Each wafer has the desired cooling passage geometry photo-etched in its surface. The wafers are then diffusion-bonded together using Transient Liquid Phase (TLP^{TM}*) bonding. The final airfoil endwalls, and internal plenum are machined from the bonded block to produce the finished turbine blade or vane with integral cooling passages of any desired complexity.

In turbine vane applications, the wafers can be oriented either radially or horizontally. For turbine blade applications, the wafers are oriented in a radial direction so the high centrifugal stresses are carried by the parent material wafers instead of the bond joints. A radial orientation was also selected for this vane design because it is more amenable to full (100%) coverage film cooling and corresponds to recent P&WA efforts. This orientation also results in a structurally stronger airfoil and simpler construction, since the endwall cooling design can be included in the same wafers that form the airfoil.

The vane design parameters and external aerodynamic profile were supplied by NASA Lewis Research Center (LeRC). The cooling design and analysis of the vane and endwalls were made by several computerized analytical procedures, programmed for use on an IBM 370 digital computer by the Pratt & Whitney Aircraft Group Government Products Division (P&WA/GPD). The analysis consists of programs for the computation of airfoil external heat transfer coefficients, adiabatic wall temperatures for both non-film cooled and film cooled conditons, internal convective heat transfer coefficients, internal coolant pressure loss and temperature rise, and metal temperature and stress-strain distributions for both transient and steady-state conditions.

Two vanes incorporating the final cooling design were fabricated by photo etching the design cooling configuration on radially oriented wafers, bonding the wafers to form a block, and then electro-discharge machining the block to the final airfoil-endwall configuration.

*TLP bonding is a P&WA process for joining superalloys. The process achieves near parent metal strength but requires only moderate bonding pressures of 15 to 20 psi, compared to conventional diffusion bonding pressures, which are generally in excess of 2000 psi.

III. DESIGN CONDITIONS

The design conditions selected were representative of the first-stage turbine stator of an advanced commercial, energy-efficient engine. In addition, the performance of the final vane design was evaluated at selected operating conditions of the NASA "One Vane Tunnel" which are representative of an advanced high temperature engine. These conditions are:

	Commercial Engine Design (Design Conditions)	*NASA "One Vane Tunnel" (Off-Design Conditions)*
Inlet Gas Stream Temp, °C (°F)	1538 (2800)	1927 (3500)
Inlet Gas Stream Pressure N/M^2, (psia)	4.14×10^5 (600)	2.76×10^5 (400)
Inlet Gas Stream Critical Velocity Ratio	0.235	0.235
Exit Gas Stream Critical Velocity Ratio	0.80	0.80
Equivalent Gas Stream Flowrate/Passage, kg/sec (lbm/sec)	0.136 (0.30)	0.136 (0.30)
Coolant Inlet Temperature, °C (°F)	649 (1200)	538 (1000)
Coolant Flowrate Goal, %	5.0	5.0

Figure 1 shows the vane external profile and coordinates which were defined by NASA LeRC. The critical velocity ratio distribution for this airfoil profile is shown in figure 2 and is the result of both an analytical and an experimental study at NASA LeRC (ref. 1). Because of the anticipated gas stream flow characteristics in the "One Vane Tunnel," a flat gas temperature profile was assumed to exist at the inlet to the turbine vane.

During the initial phase of the design effort, a coolant inlet temperature of 704°C (1300°F) was specified. It became apparent, however, that this was too severe to result in an acceptable cooling scheme without utilizing film cooling in the high Mach number recovery region of the suction surface. Discussions with the NASA Program Manager indicated that the aerodynamic penalties of film cooling the suction surface were unacceptable and that a convection cooling scheme should be used. A relaxation of the coolant flowrate goal of 5% and a reduction in coolant inlet temperature to 649°C (1200°F) were permitted to facilitate an acceptable suction surface cooling scheme without film cooling. For both conditions the coolant supply pressure was assumed equal to approximately 1.05 times the inlet gas stream pressure.

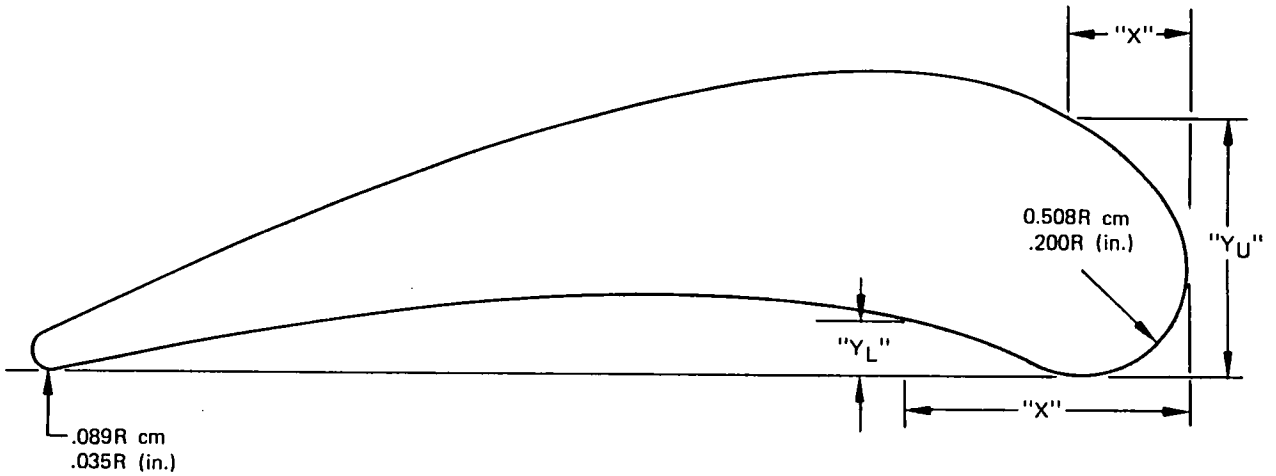

X		Y_L		Y_U	
(in.)	(cm)	(in.)	(cm)	(in.)	(cm)
0.0	0.0	0.200	0.51	0.200	0.51
0.050	0.131			0.335	0.85
0.100	0.25			0.396	1.01
0.150	0.38			0.442	1.12
0.200	0.51			0.478	1.21
0.250	0.64			0.507	1.29
0.300	0.76	0.025	0.06	0.530	1.37
0.350	0.89	0.047	0.12	0.548	1.39
0.400	1.02	0.065	0.17	0.562	1.43
0.450	1.14	0.081	0.21	0.572	1.45
0.500	1.27	0.095	0.24	0.578	1.47
0.550	1.40	0.105	0.27	0.580	1.47
0.600	1.52	0.115	0.29	0.581	1.48
0.700	1.78	0.130	0.33	0.576	1.46
0.800	2.03	0.142	0.36	0.564	1.43
0.900	2.29	0.148	0.38	0.544	1.38
1.000	2.54	0.151	0.38	0.521	1.32
1.100	2.79	0.150	0.38	0.495	1.26
1.200	3.05	0.147	0.37	0.468	1.19
1.300	3.30	0.139	0.35	0.437	1.11
1.400	3.56	0.130	0.33	0.406	1.03
1.500	3.81	0.117	0.30	0.372	0.94
1.600	4.06	0.103	0.26	0.335	0.85
1.700	4.32	0.087	0.22	0.294	0.75
1.800	4.57	0.071	0.18	0.251	0.64
1.900	4.83	0.052	0.13	0.204	0.52
2.000	5.08	0.032	0.08	0.154	0.39
2.100	5.33	0.010	0.02	0.102	0.26
2.186	5.55	0.035	0.09	0.035	0.09
	LER	0.200	0.51		
	TER	0.035	0.09		

FD 162721

Figure 1. NASA Vane External Profile

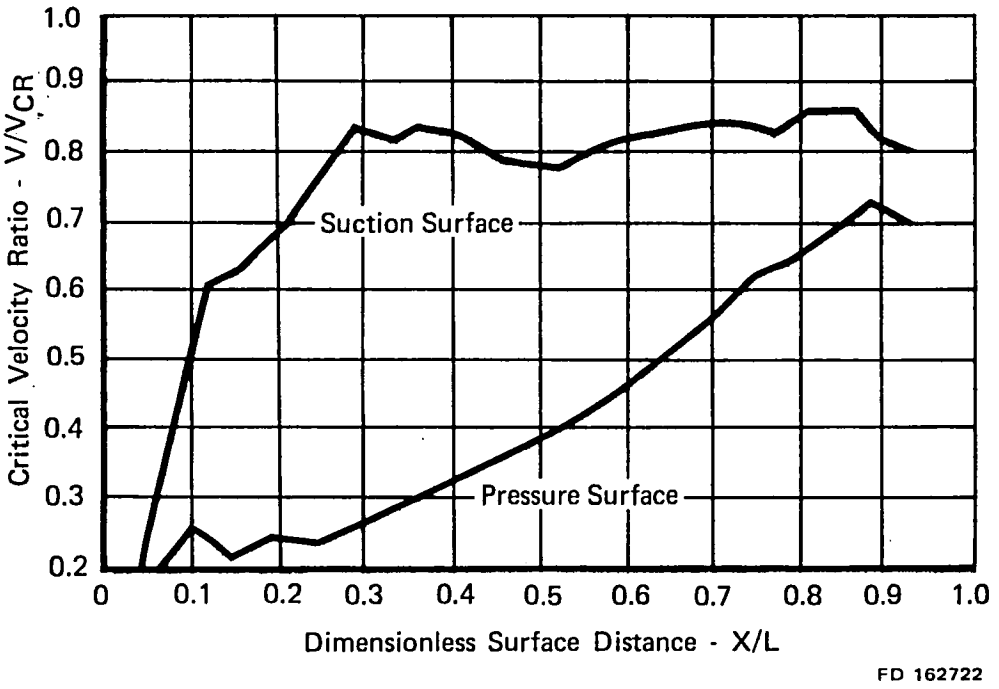

Figure 2. NASA Vane Critical Velocity Ratio

IV. DESIGN DESCRIPTION

A. GENERAL

The objective of the thermal analysis was to establish an effectively cooled turbine vane airfoil and endwalls for the stated design conditions using the radial wafer concept. After a given design was established, a detailed thermal analysis of the entire structure was performed. The P&WA/GPD thermal and durability analyses are composed of several computerized analytical procedures programmed for use on an IBM 370 digital computer. These analyses consist of programs for the computation of airfoil external heat transfer coefficients, adiabatic wall temperatures for both film cooled and nonfilm cooled airfoils, internal convective heat transfer coefficients, internal coolant pressure loss and temperature rise, metal temperature distribution, stress-strain relationship, and the creep-rupture life analysis. Analyses are capable of handling both transient and steady-state conditions.

The design procedure utilized for the endwall analysis was somewhat less rigorous than the vane airfoil analysis. Because the flow field in the endwall region is highly three dimensional, a detailed design procedure equivalent to the two dimensional procedure for the airfoil has not presently been established. Several endwall investigations have been conducted and are currently being conducted both within P&WA and by other companies or government agencies. The empirical results of the P&WA investigations have been utilized to assist in defining endwall cooling design.

B. THERMAL ANALYSIS

The external heat transfer coefficients were obtained using the P&WA-developed computational procedure (ref. 2). In this boundary layer program a general finite-difference procedure for computing the behavior of compressible two-dimensional boundary layers is utilized together with a turbulence model which allows quantitative predictions of the location and extent of the transition region between laminar and turbulent flow as it is influenced by such disturbances as surface roughness and free-stream turbulence. Reverse transition, i.e., relaminarization, caused by large favorable streamwise accelerations, is also quantitatively predicted by this procedure. The solution procedure depends upon the calculation of the streamwise development of a turbulent mixing length whose magnitude is governed by the turbulence kinetic energy equation. A large number of comparisons between predictions and measurements have been made with this program and, in general, very good agreement is obtained.

A separate film cooling program is used to calculate film temperatures for airfoils with showerhead and/or aft section film cooling. Figure 3 presents the model used for the definition of heat transfer and film effectiveness. The film temperatures are based on correlations between cascade test data and an empirical model for multihole cooling. This is further supplemented by the basic wafer slot film effectiveness tests conducted at the United Technologies Research Center. Film temperatures along the airfoil surface are calculated using a driving potential defined as the difference between the coolant ejection temperature and the mainstream gas temperature. Figures 4 and 5 present the film effectiveness curves for the showerhead and pressure side sections, respectively.

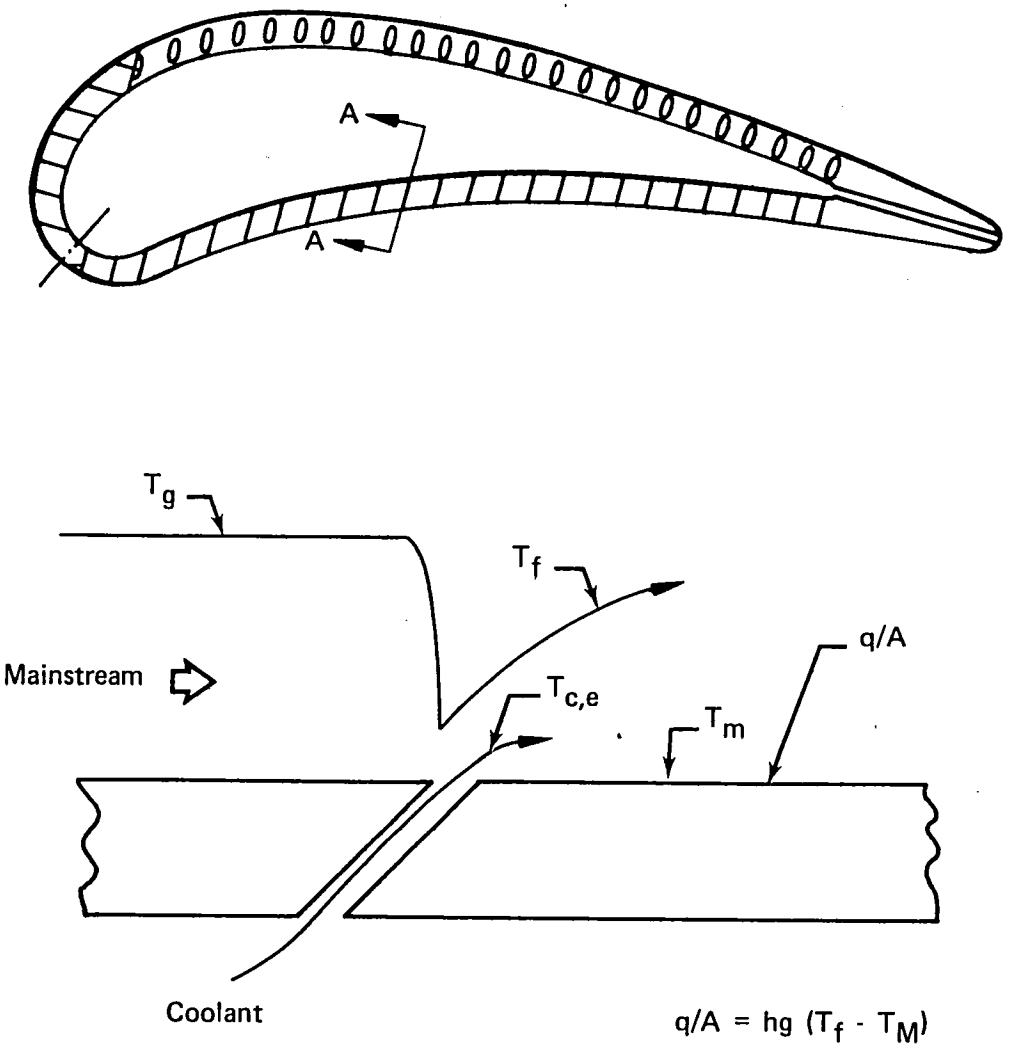

Figure 3. Heat Transfer and Film Effectiveness Model

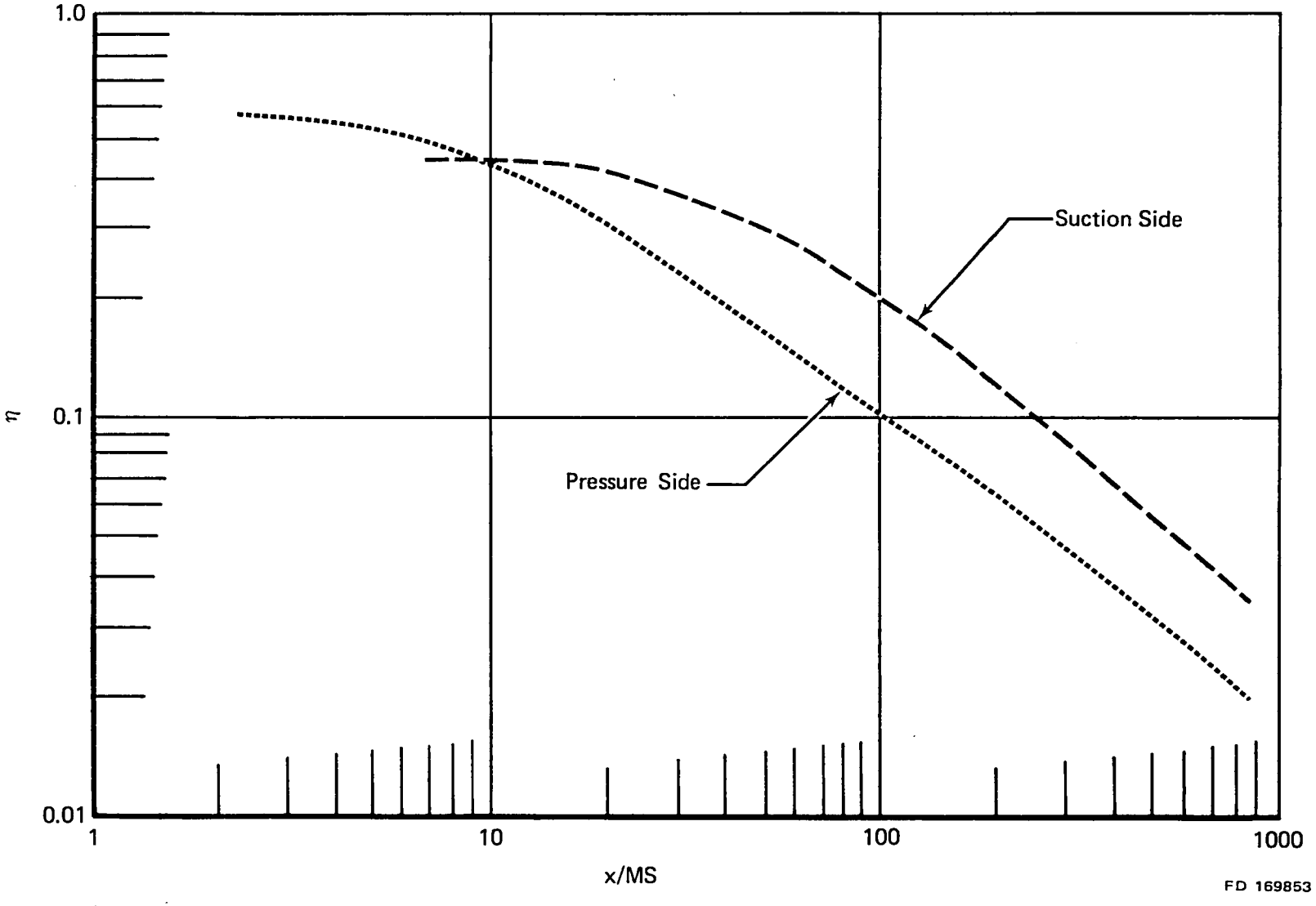

Figure 4. Leading Edge Film Effectiveness

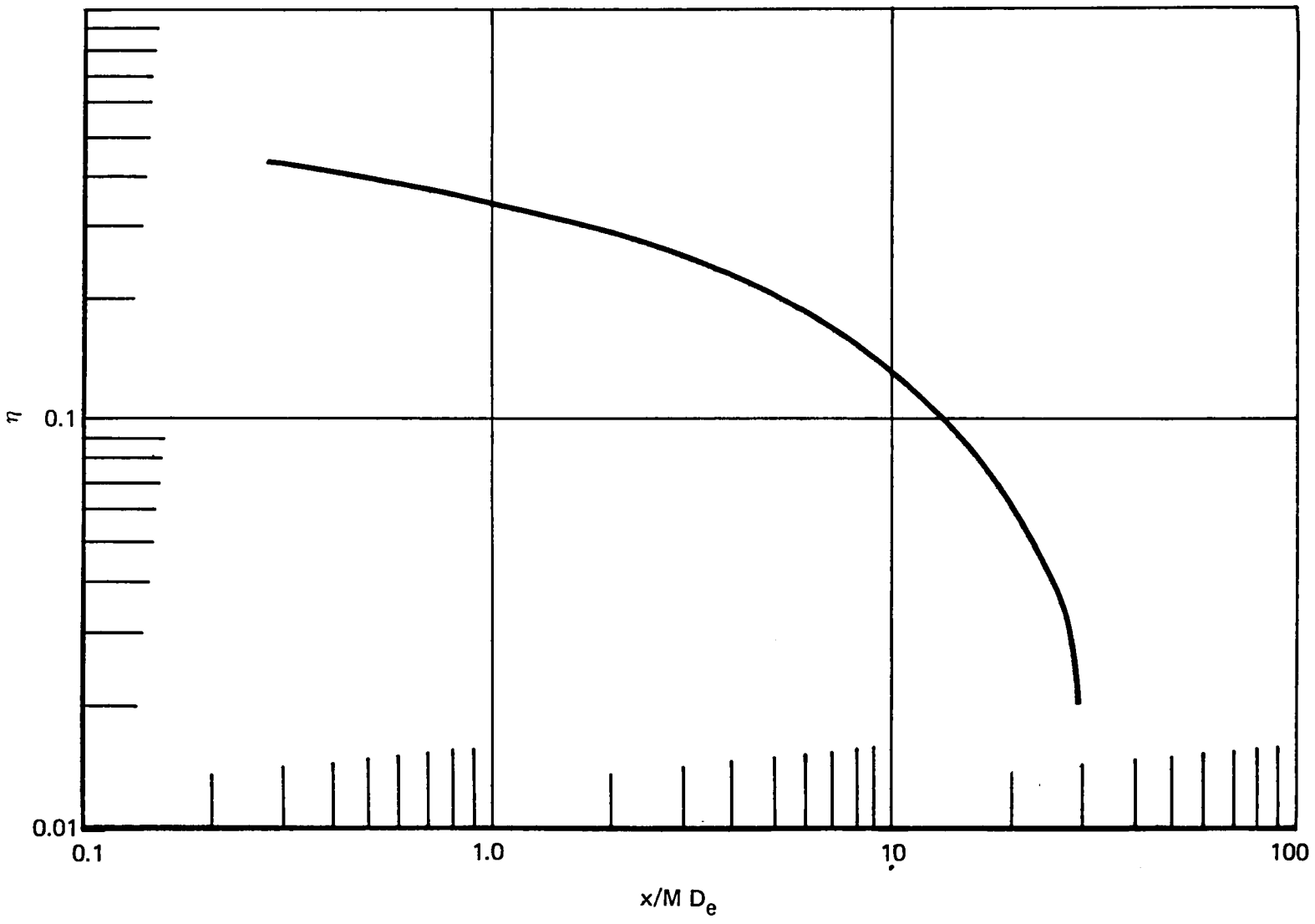

Figure 5. Pressure Side Film Effectiveness

The airfoil coolant-side analysis provides detailed heat transfer, pressure drop, and flow distribution information. This is accomplished by the analysis of compressible flow through multiple channels with multiple exits and variable flow conditions. This analysis is a general purpose computer program that accounts for convective heat transfer, rotational effects on total temperature and pressure, pressure losses due to bends and sudden changes in cross-sectional area, and distribution of airflow among the multiple passages. The internal heat transfer coefficients for the leading edge, pressure side, and suction side were obtained using the Colburn turbulent flow equation, (ref. 3). For the trailing edge section, the coefficients were defined based on tests conducted by P&WA for the wavy crisscross pattern. The computer solution for the flow distribution was further adjusted by the experimental cold flow results from several P&WA radial wafer airfoil designs and the AFAPL radial wafer vane program (ref. 4). The modifications consisted of defining a friction factor for the etched passages based on the previous experimental results.

The predicted cold flow characteristics for the vane and the end-walls are also determined using the experimentally adjusted computer deck. For the cold flow study, however, a static discharge pressure of ambient is assumed, heat transfer is eliminated, and a coolant temperature of 21°C (70°F) is utilized.

A generalized heat transfer program is used to determine the airfoil transient or steady-state metal temperature distribution after defining the flow and heat transfer characteristics for both the external and internal surfaces. Initially the airfoil is broken up into sufficient elements or nodes to define the temperature distribution. In addition to conduction and convection calculations, this program accounts for radiation, internal heat generation and heat storage. Provisions are available for specifying thermal variations in properties such as specific heat, conductivity, and heat transfer coefficients, and time dependent variations in film coefficients and fluid temperatures which result in a direct solution for temperatures. This analysis is readily applicable for evaluation of convection, film, and transpiration cooling, or any combination of the three.

C. STRESS ANALYSIS

A transient cycle was not defined for the vane design other than the capability of the vane to withstand cascade testing and ten cycles from the design condition to shutdown where the vane will reach ambient temperatures. Assuming the NASA cascade shutdown cycle is a gradual decrease in conditions and not an abort type of shutdown, steady-state conditions were utilized to determine the durability of the vane.

The object of the durability analysis is to calculate elastic thermal stresses in a body or irregular shape such as turbine vane or blade which is subject to a non-uniform temperature distribution. The analysis is programmed into a computer deck which operates in conjunction with the generalized heat transfer computer deck. For durability analysis the identical nodal breakup defined for the heat transfer solution was utilized with the main input, temperature distribution being supplied from the heat transfer deck. Assuming no external restraint will prevent the body from expanding freely, a system of simultaneous equations is developed that represents the internal interference of one fiber or node of the

body with another. These equations must satisfy the following conditions: (1) the sum of the internal interference forces must be zero; (2) the moment of internal stresses about any two arbitrarily chosen axes that are mutually perpendicular must also be zero. The following assumptions are also inherent to the analysis:

a. Elastic behavior of the body is assumed

b. The body cross section remains plane even after heating and subsequent elongation and bending

c. The cross section is not near the ends of the body so that boundary effects need not be included

d. The elements of the body are considered thin-walled so that stresses perpendicular to the wall of the body can be neglected (i.e., Poisson Ratio effects are non-existent).

The durability analysis included: (1) low-cycle fatigue life, (2) creep-stress rupture life, (3) vane suction side bulging study, and (4) oxidation/erosion life.

D. MATERIAL SECTION

The material selected for the vane and endwalls was Mar-M 200 +Hf (PWA 1422). This same material is currently used by P&WA in the first stage turbines for both the government (F100) and commerical (JT9D) engine applications. Although other advanced materials such as single crystal and TD-nickel were considered, lack of etching and bonding experience for the single crystal material and unacceptably high oxidation characteristics of the TD-nickel eliminated these two materials. Also due to the high utilization of PWA 1422 in P&WA advanced engines, detailed material characterization work, and the fact that one radial wafer airfoil had been fabricated with this material, it was deemed the best material available for the design.

V. RESULTS OF DESIGN

A. VANE DESIGN THERMAL RESULTS

The design study was initiated with the determination of the external heat transfer coefficients as discussed previously in Section IV. The coefficients for both the design and off-design points are shown in figure 6. The vane external contour and pressure profile utilized to define the coefficients were presented previously in Section III.

The final design is separated into four sections that consist of the leading edge, pressure side, suction side, and trailing edge. The predicted internal coolant flow distribution for each section is shown in figure 7 for the design conditions. The total coolant flow to the vane is 6.17% of the gas stream flow.

The predicted cold flow parameters for the total vane, endwalls, and each of the four sections are presented in figures 8 through 13. These cold flow parameters for the vane, endwalls, and each of the four sections of the vane were determined analytically utilizing the airfoil coolant-side analysis deck. The cooling flow circuits used in the analysis for the vane and endwall are presented in figure 14. The curves were generated by varying the coolant flowrate over a range consistent with the particular section in question and solving for the corresponding supply pressure while assuming a coolant temperature of 21°C (70°F) and discharging to a constant ambient pressure of 10.1×10^3 N/M^2 (14.7 psia). The design point pressure ratio included on figures 10 through 13 refer to the coolant supply total pressure divided by the average discharge static pressure at the design point conditions. This parameter is omitted from figures 8 and 9 due to the wide range in discharge static pressures associated with the entire vane and endwalls.

The final passage dimensions required to obtain the desired coolant flow split are shown in figure 15. Included on the figure are the suction side and pressure side wall thicknesses. The transition in thickness from suction side to pressure side occurs gradually through the leading edge showerhead section. A detailed description of each of the four sections is presented in the following paragraphs.

The leading-edge section consists of a ten row showerhead array with nine etched rows and one electrical discharge machined (EDM) row. The EDM row is located near the stagnation region and is required to provide film cooling where no wafer interface exists. The etched rows are split into three rows on the pressure side and six rows on the suction side. The increased number of rows on the leading-edge suction side is required to provide sufficient cooling effectiveness in the downstream high Mach number region to assist in cooling the suction side. As stated previously, ejection of film cooling air in this region was eliminated because of the high aerodynamic penalties.

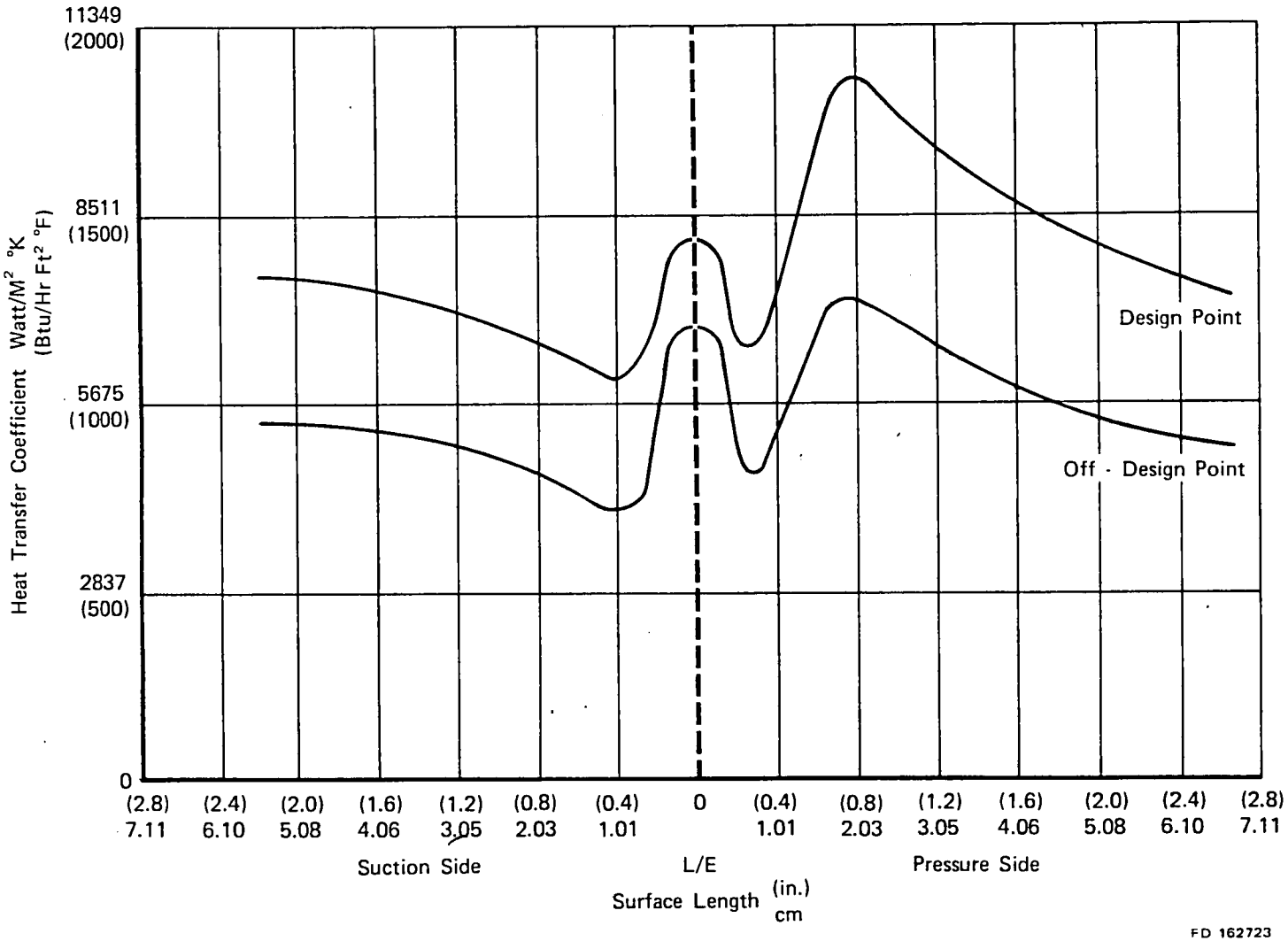

Figure 6. NASA Radial Wafer Vane Heat Transfer Coefficient Distribution

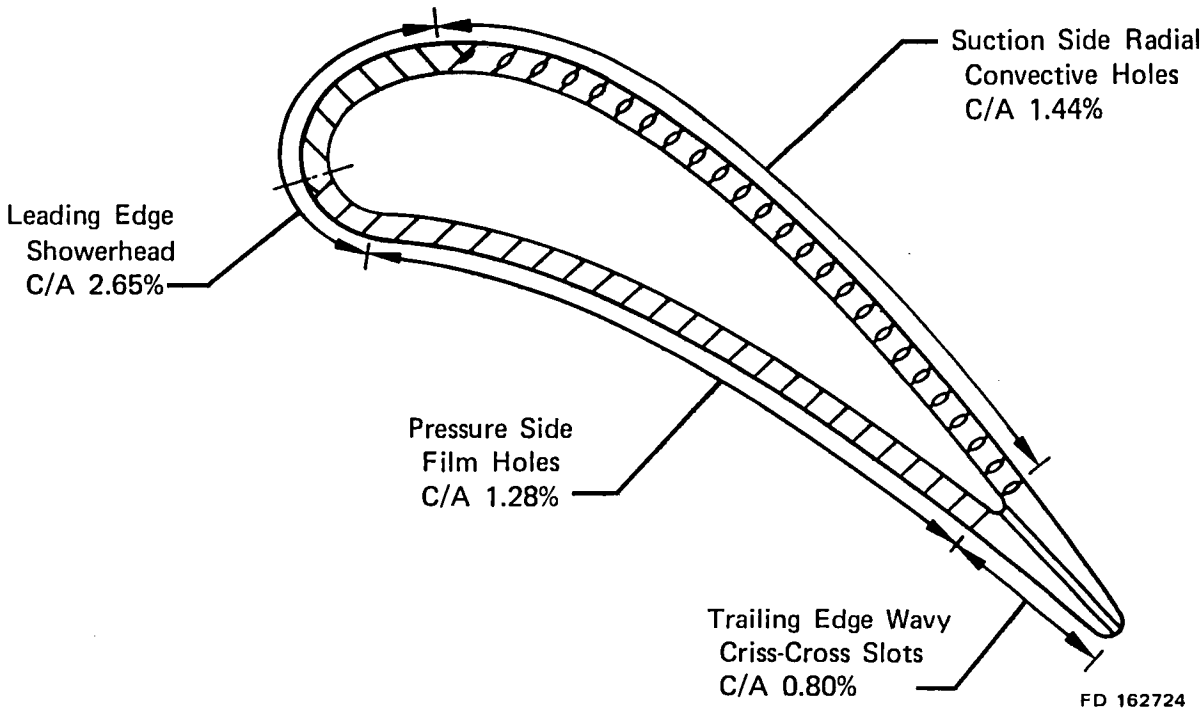

Figure 7. NASA Radial Wafer Vane Cooling Design

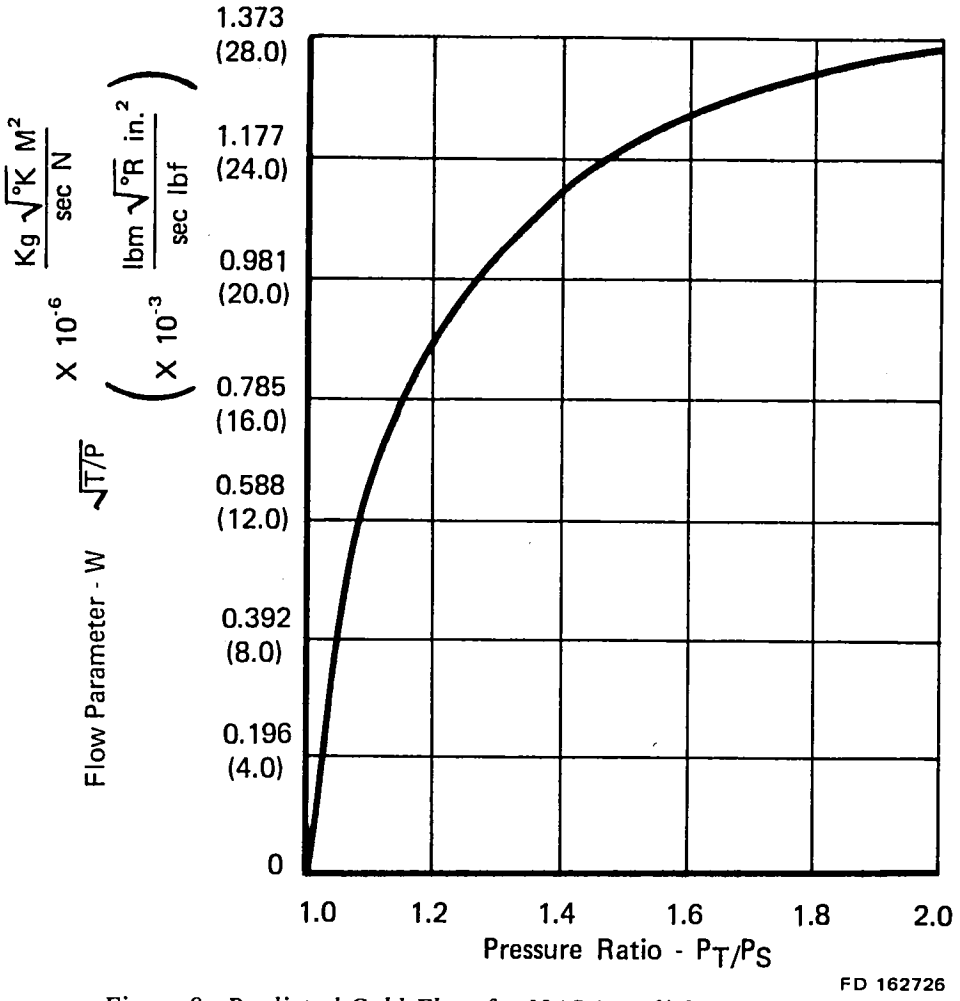

Figure 8. Predicted Cold Flow for NASA Radial Wafer Vane

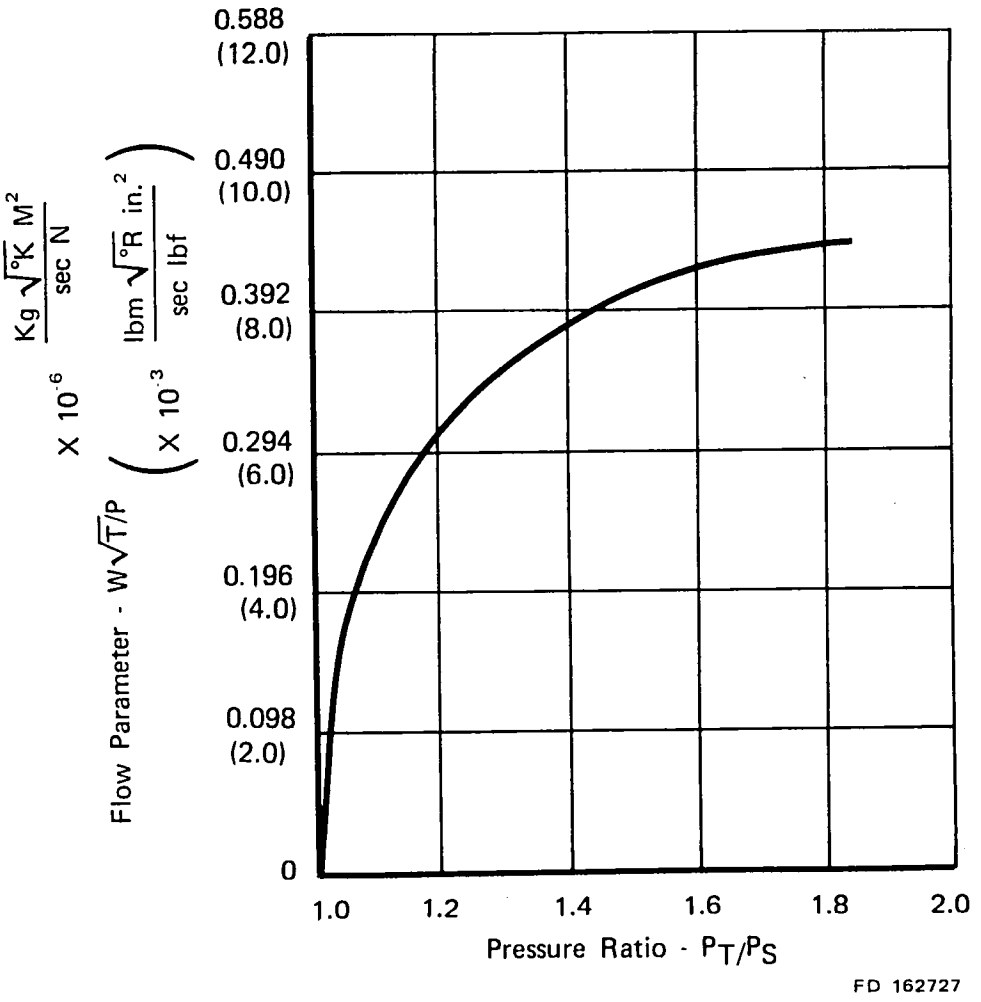

Figure 9. Predicted Cold Flow for NASA Radial Wafer Vane - Endwall

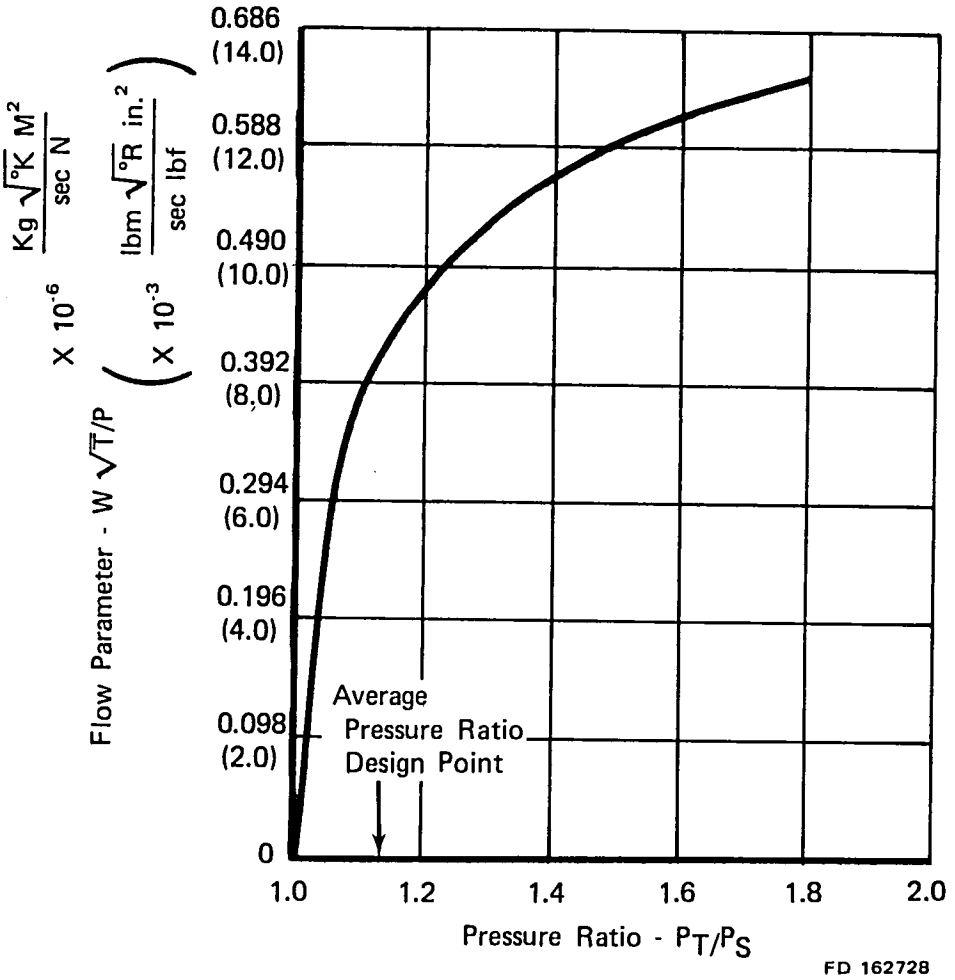

Figure 10. Predicted Cold Flow for NASA Radial Wafer Vane - Leading Edge Section

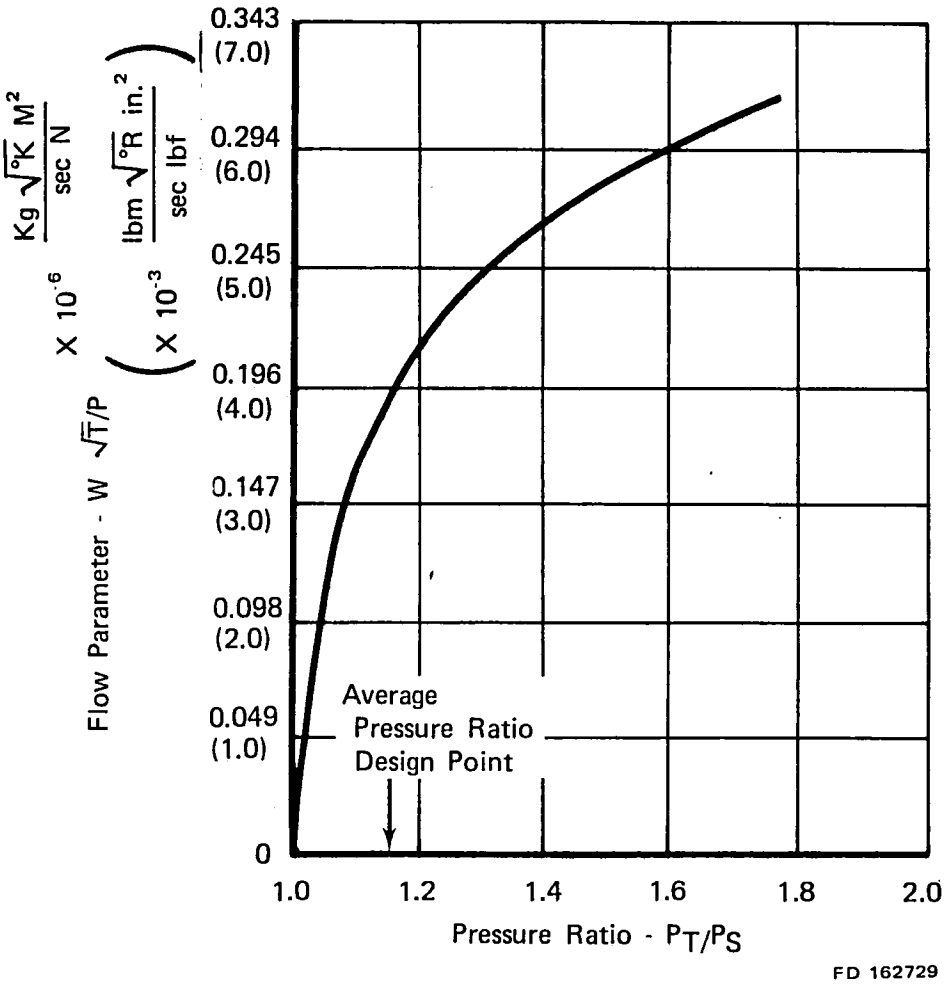

Figure 11. Predicted Cold Flow for NASA Radial Wafer Vane - Pressure Side

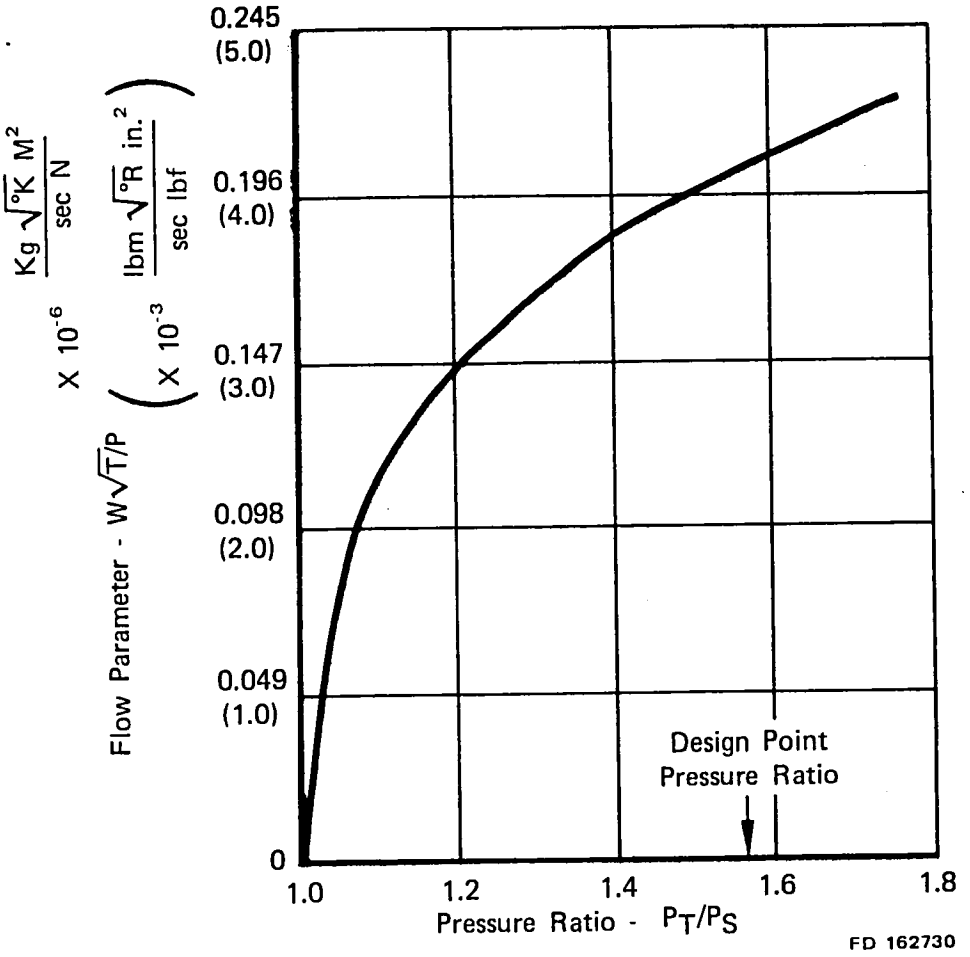

Figure 12. Predicted Cold Flow for NASA Radial Wafer Vane - Suction Side

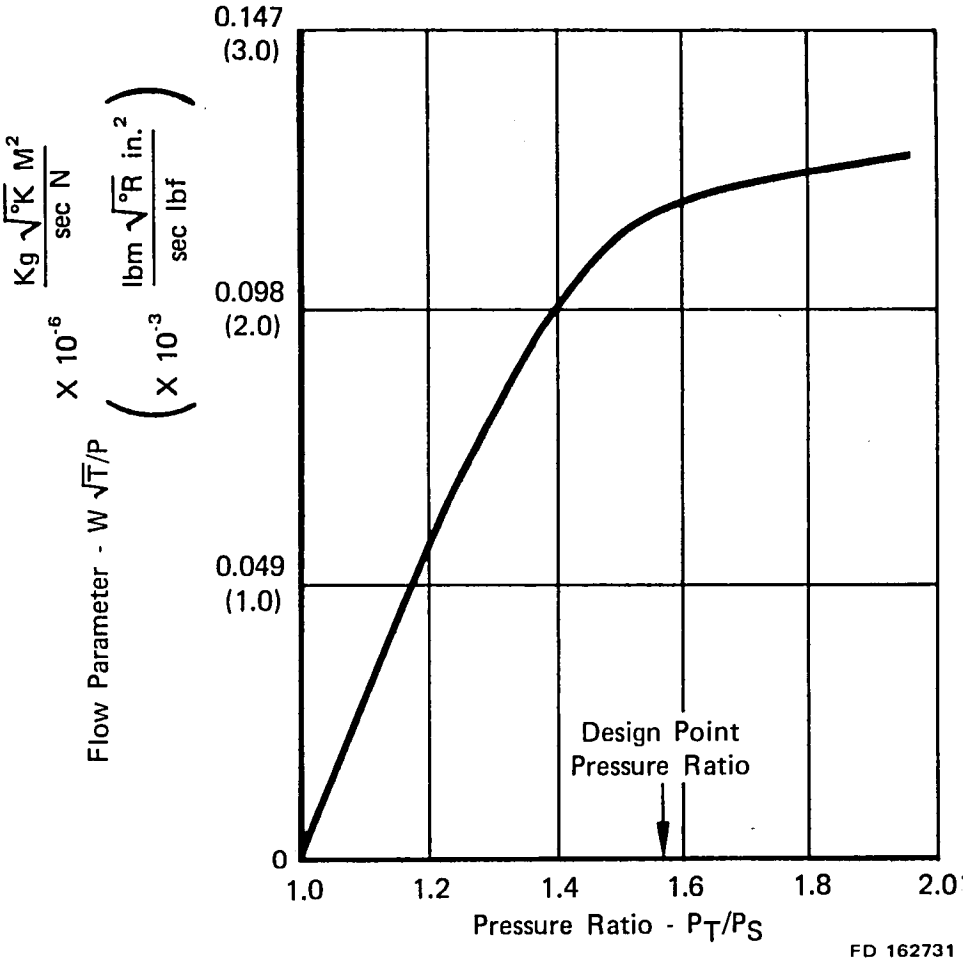

Figure 13. Predicted Cold Flow for NASA Radial Wafer Vane - Trailing Edge

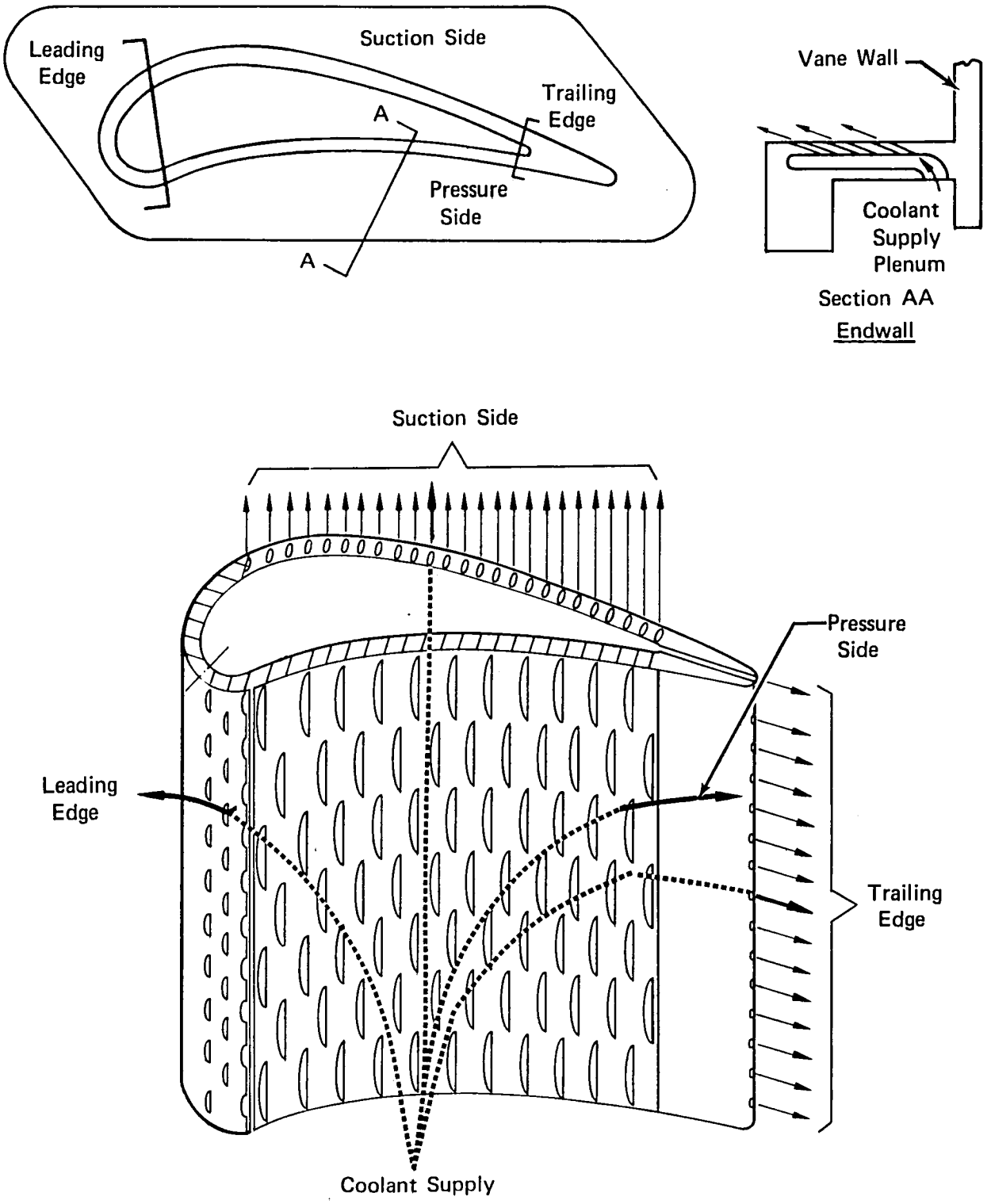

Figure 14. Coolant Flow Circuits for Vane and Endwall

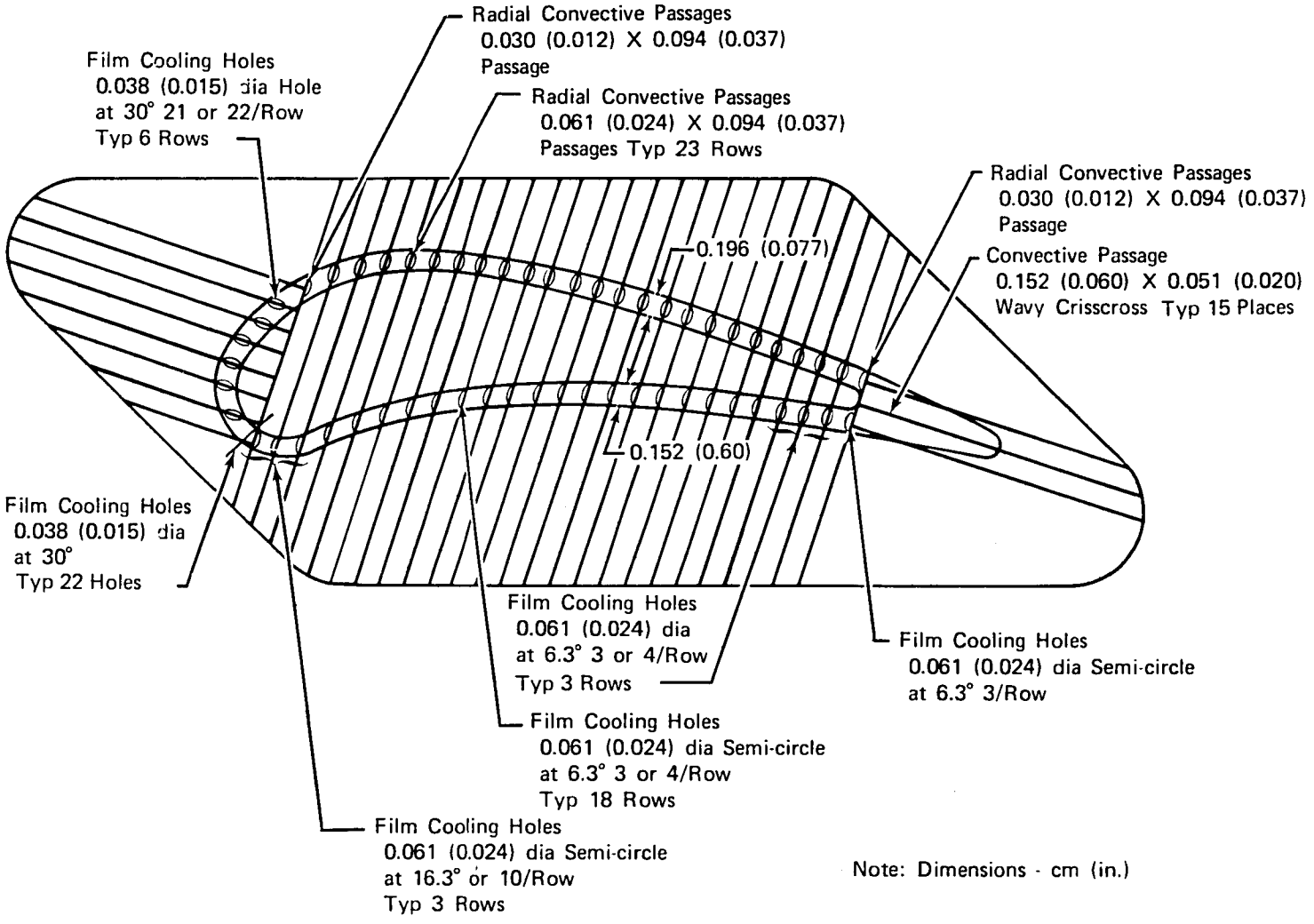

Figure 15. NASA Radial Wafer Vane Cooling Geometry

Radial film cooling injection angles rather than normal injection angles were used on the leading edge for two reasons. The first reason is to increase the coolant side convective heat transfer. A radially angled film cooling hole will increase the passage length through the wall relative to film cooling hole with a normal angle. This increase in length will increase the coolant side convective heat transfer area and thereby increase the convective heat transfer. The second reason for angling the hole is to increase the film effectiveness. An angled passage results in less penetration and mixing of the coolant jet into the mainstream than a normal passage based on tests conducted by P&WA. In addition, angling the hole also results in the breakout area of the passage on the surface of the airfoil being greater than a normal passage. Both effects result in an increase in film effectiveness when compared to a normal passage. The film passages are also staggered from row to row to provide full coverage film cooling.

The pressure side film cooling design is also a radially angled passage - staggered row cooling scheme. As illustrated in figure 15, the passages are etched into one side of the wafer except for the three rows preceding the last row. In this region the wafers are etched on both sides to double the flow area which will increase the flowrate in that region and increase the film effectiveness. This was done to assist in cooling the convectively cooled trailing edge section.

The suction side utilizes a simple oval shape radial convective passage. The coolant is used first to cool the suction side then collected in a tip plenum for additional cooling of the blade rub strip or the platform. Double use of the coolant in this manner is a potential means to increase engine cycle efficiency by reducing the total amount of coolant required.

The cooling design for the trailing edge section is the wavy crisscross slot geometry. The design is an extremely efficient convective cooling technique which was used on the AFAPL radial wafer vane design (ref. 4). Because the wafers which form the trailing edge passage are bonded in the plane of the trailing edge slot, each wafer has half the passage geometry. The passage for each half is sinusoidal and the two sine waves are 180 deg out of phase with respect to each other. Therefore, they are continually crossing one another along the trailing edge slot.

The vane nodal breakup is shown in figure 16. This breakup is relatively detailed in that four temperatures are defined to supply the temperature gradient through the wall. Figure 17 shows the predicted film temperature distribution for the design and off-design points.

The predicted vane outside wall temperature profiles for the design point and the off-design point are shown in figures 18 and 19, respectively. A tabulation of the temperature and surface distances for the two points is included in Appendix A. For the design point the maximum (hot spot) temperature was 1059°C (1939°F) on the suction side near the trailing edge. The temperature is below the design life requirement of 1079°C (1975°F). The figures also indicate an overcooled section of the suction side near the leading edge. This was caused by discharging a relatively large amount of cooling air in this region to assist in cooling the suction side of the vane. This extra cooling was required because film cooling along the suction side was not desired due to the aerodynamic penalties associated with film cooling in a relatively high velocity area.

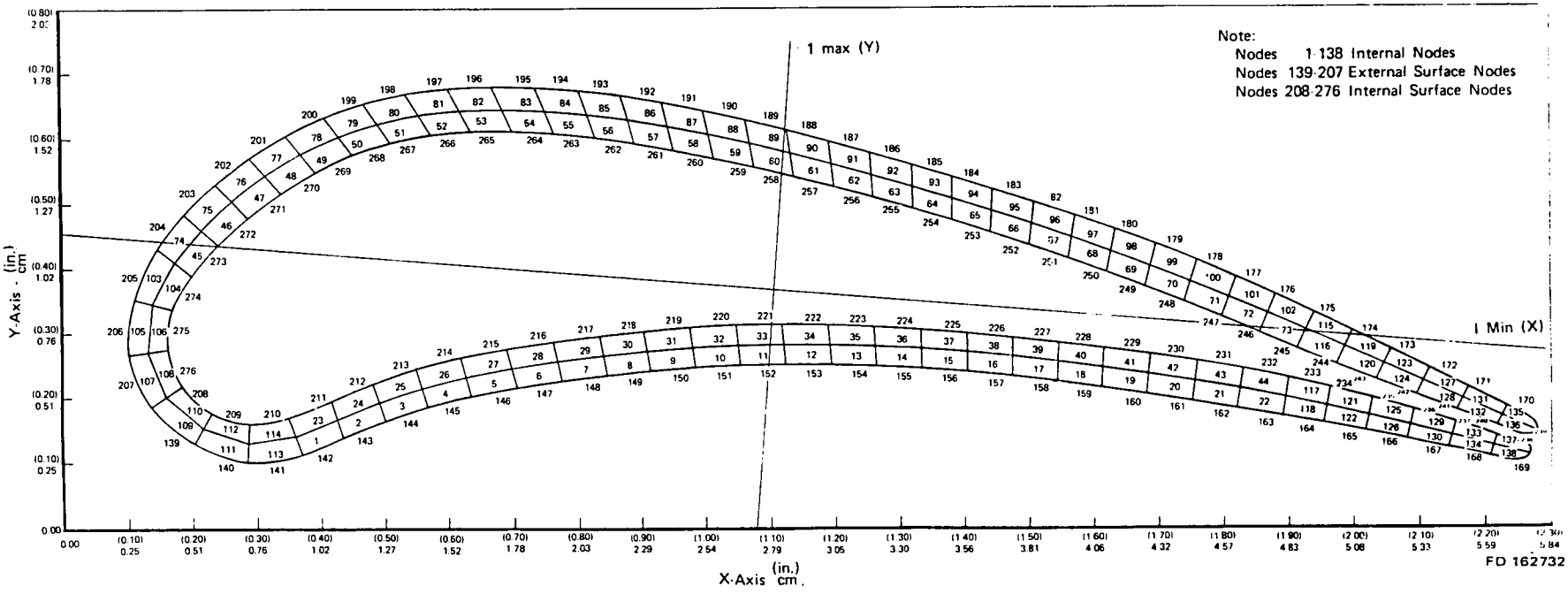

Figure 16. Detailed Nodal Breakup of the Radial Wafer Vane

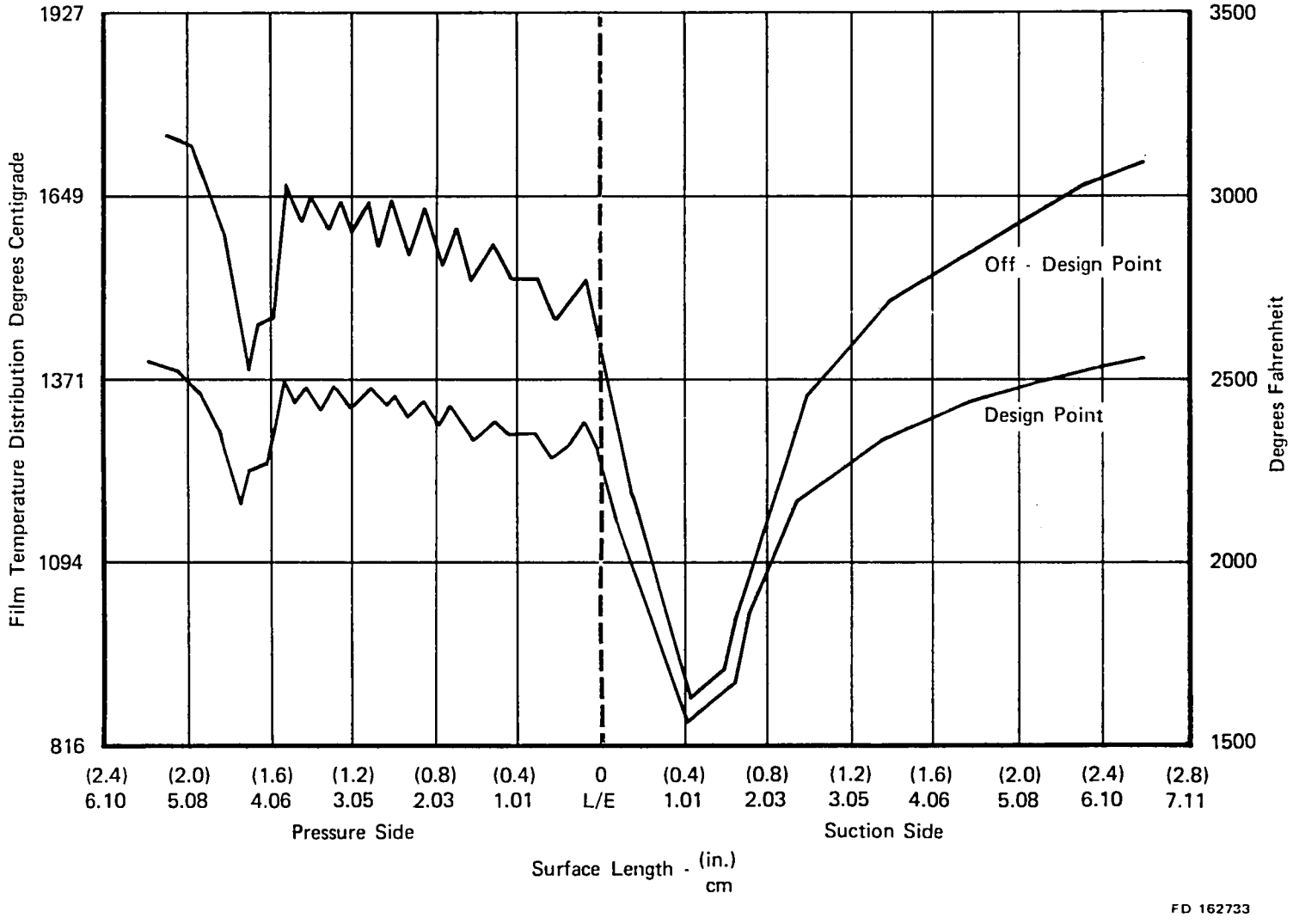

Figure 17. NASA Radial Wafer Vane External Film Temperature Distribution

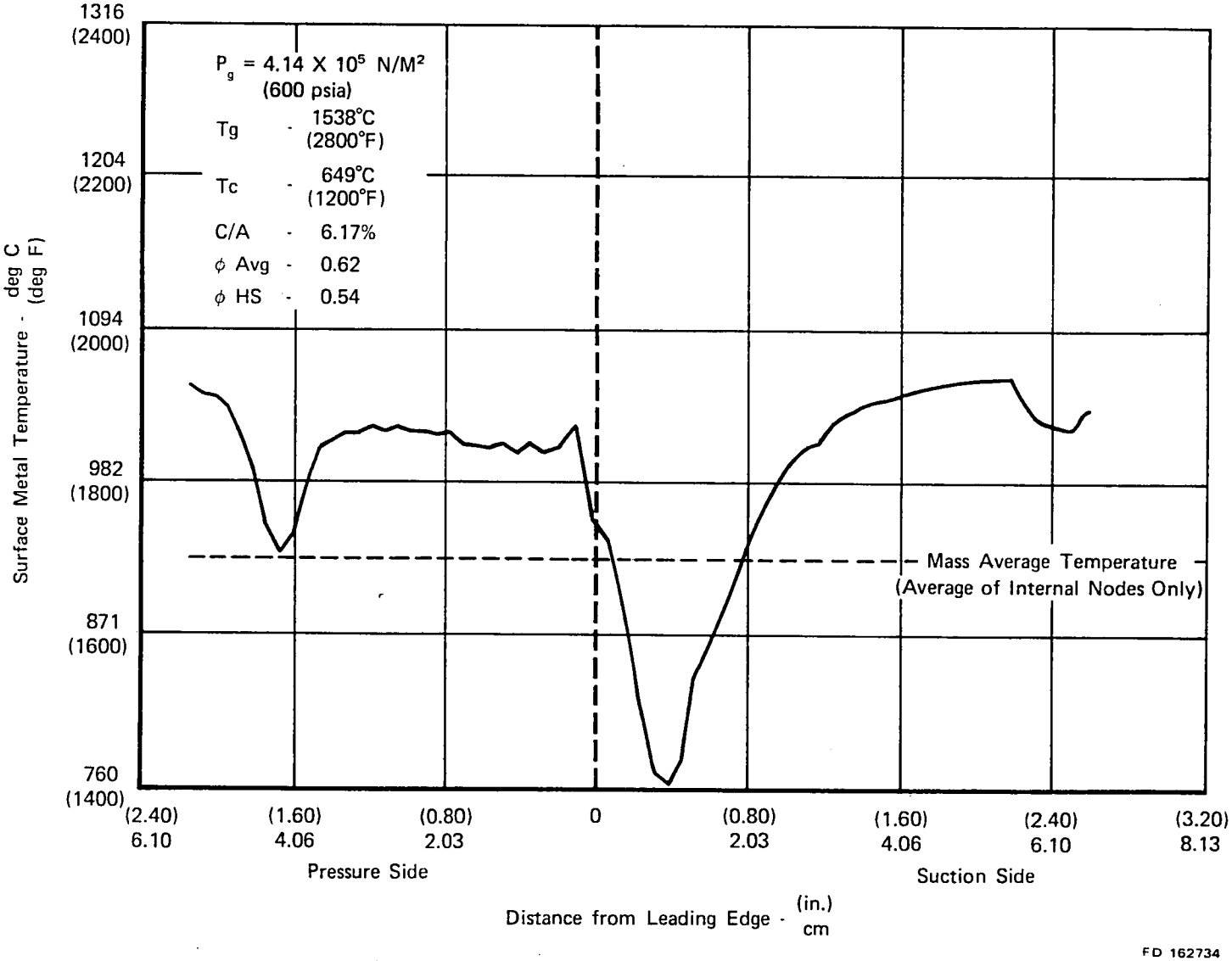

Figure 18. NASA Radial Wafer Vane - Temperature vs Surface Distribution for Design Point

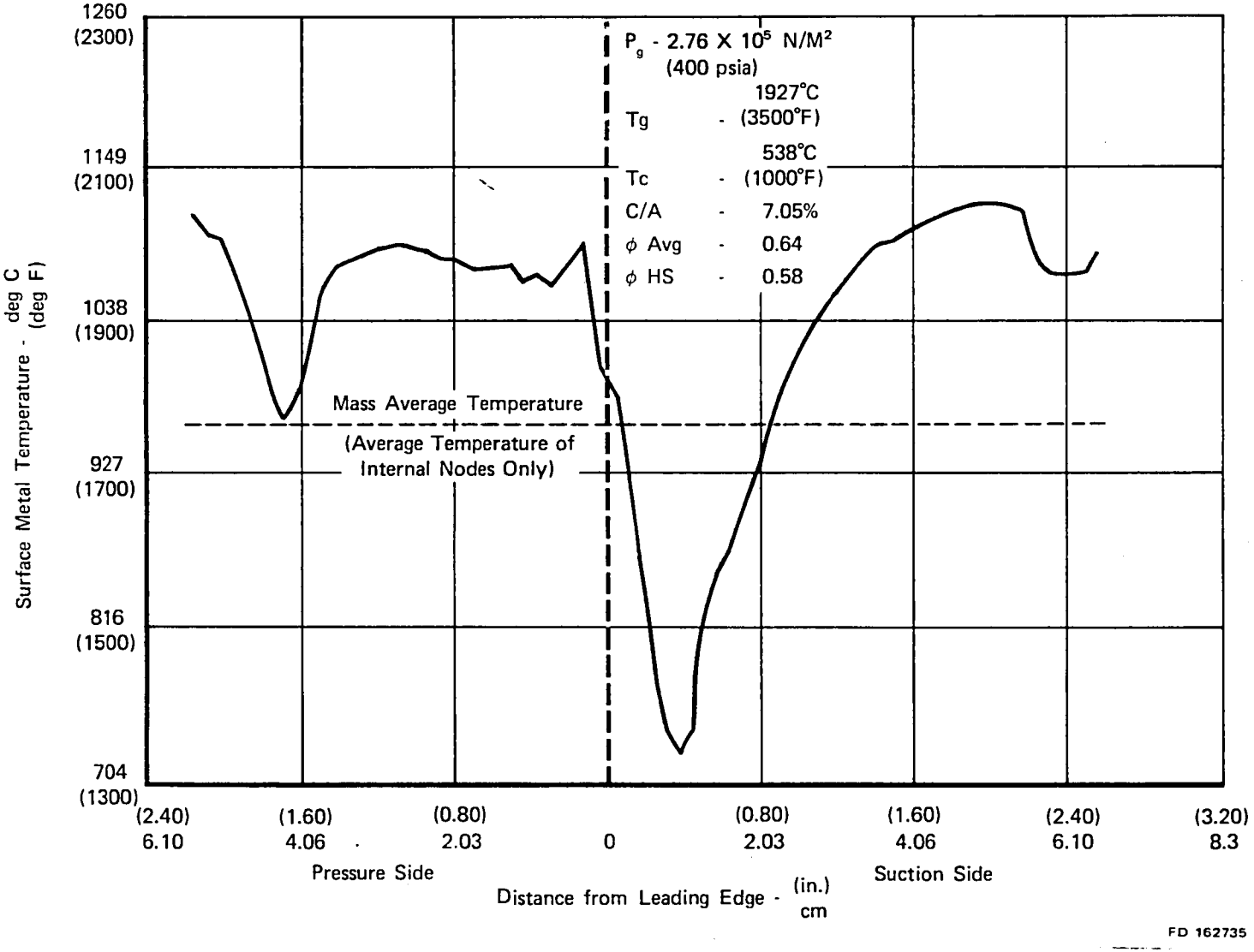

Figure 19. NASA Radial Wafer Vane - Temperature vs Surface Distribution for Off-Design Point

B. VANE DESIGN DURABILITY RESULTS

1 Low Cycle Fatigue Life

Low cycle fatigue (LCF) life is normally determined based on the percent strain range developed during a transient cycle such as idle to sea level take-off. For this program, however, no transient cycle was defined since the design will be evaluated in a steady-state heat transfer cascade rig. It was therefore decided to base the LCF life on the percent strain range developed at the two design points.

Although no LCF tests have been performed on etched and bonded wafer passages with PWA 1422 material, tests have been conducted with PWA 1401 material and astrology. Results from these tests have indicated the wafer samples exhibited LCF characteristics equal to that of the solid material. Because of the results obtained with the other materials and since LCF testing of wafered PWA 1422 material was beyond the scope of this program, the LCF life curve for solid PWA 1422 material was utilized.

Maximum strain ranges of 0.32 and 0.46% were developed for the design and off-design points respectively. This results in predicted cyclic life of approximately 10^5 and 10^4 cycles as shown by the LCF life curve for PWA 1422 presented in figure 20. The location of the maximum strain range node for both design points is on the pressure side near the trailing edge as shown in figure 21 as well as some typical values around the vane contour.

2. Creep-Stress Rupture Life

The creep-stress rupture life analysis was conducted with the steady state relaxation computer program. Due to the extremely large amount of computer time required to run this deck to completion, the deck was run to determine approximately one-third of the design life. The remaining life was defined utilizing a logarithmic extrapolation method. Analysis resulted in a total life prediction of greater than 4000 hr at the design point and 500 hr at the off-design point.

3. Vane Suction Side Bulging Study

The bulging study was conducted on the vane suction side near the trailing edge which was the location where rupture failure was predicted to occur based on the creep-stress rupture analysis. The study was conducted assuming a wall thickness of 0.05 cm (0.02 in.), which is the minimum thickness between the outside wall and the convective passage. The maximum wall thickness is approximately 0.19 cm (0.077 in.); therefore, assuming an effective wall thickness of 0.05 cm should be a conservative approach. The 1.0% creep material property was utilized and the bulging life was predicted based on an empirical correlation resulting from a P&WA experimental investigation. The calculation indicated a creep-stress rupture life of 70 and 20 hr for the design and off-design points, respectively. The off-design life of 20 hr is relatively short which is a result of the high temperature, 1124°C (2056°F), and thin wall assumption associated with that location on the vane.

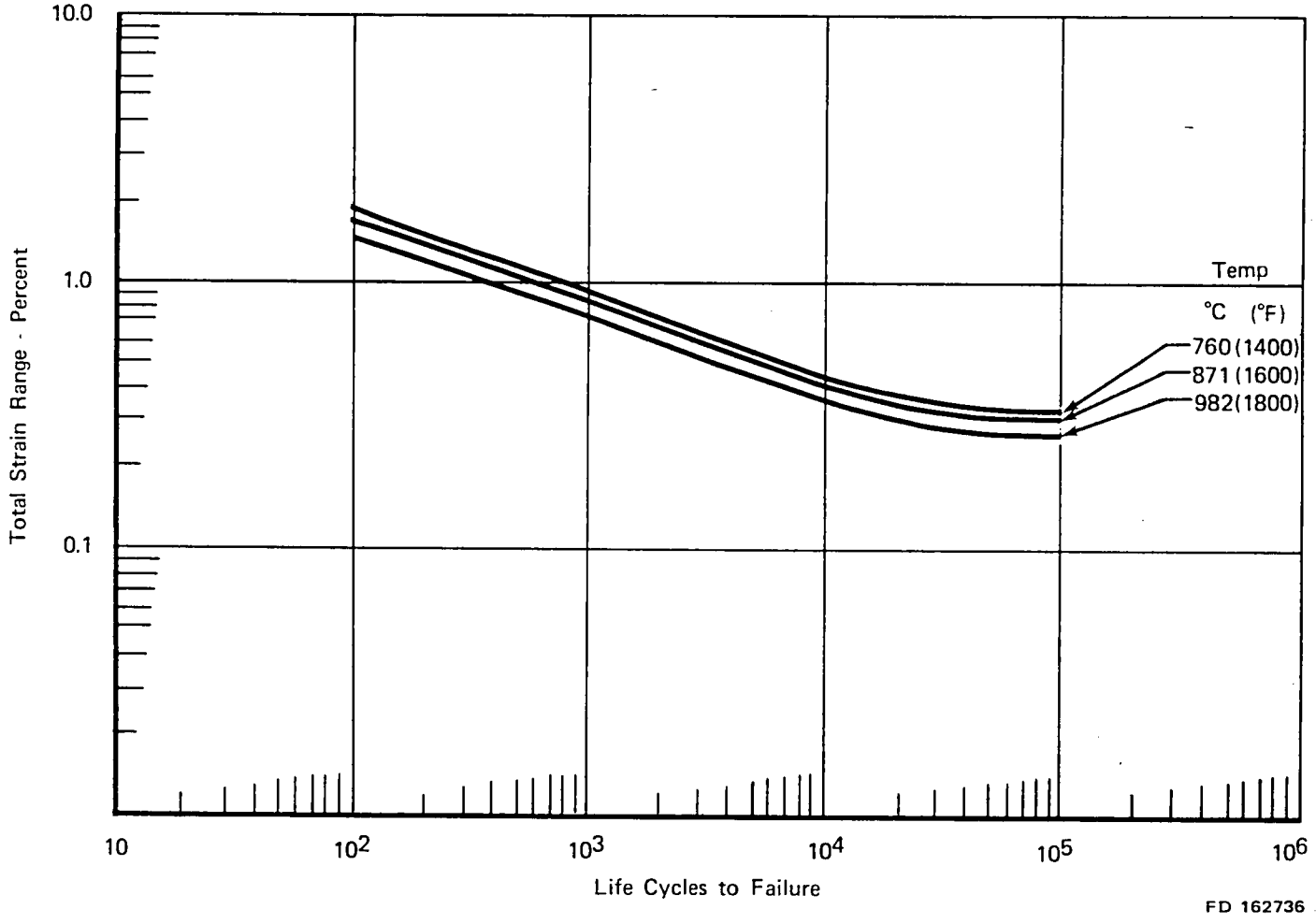

Figure 20. Low Cycle Fatigue Life for PWA 1422

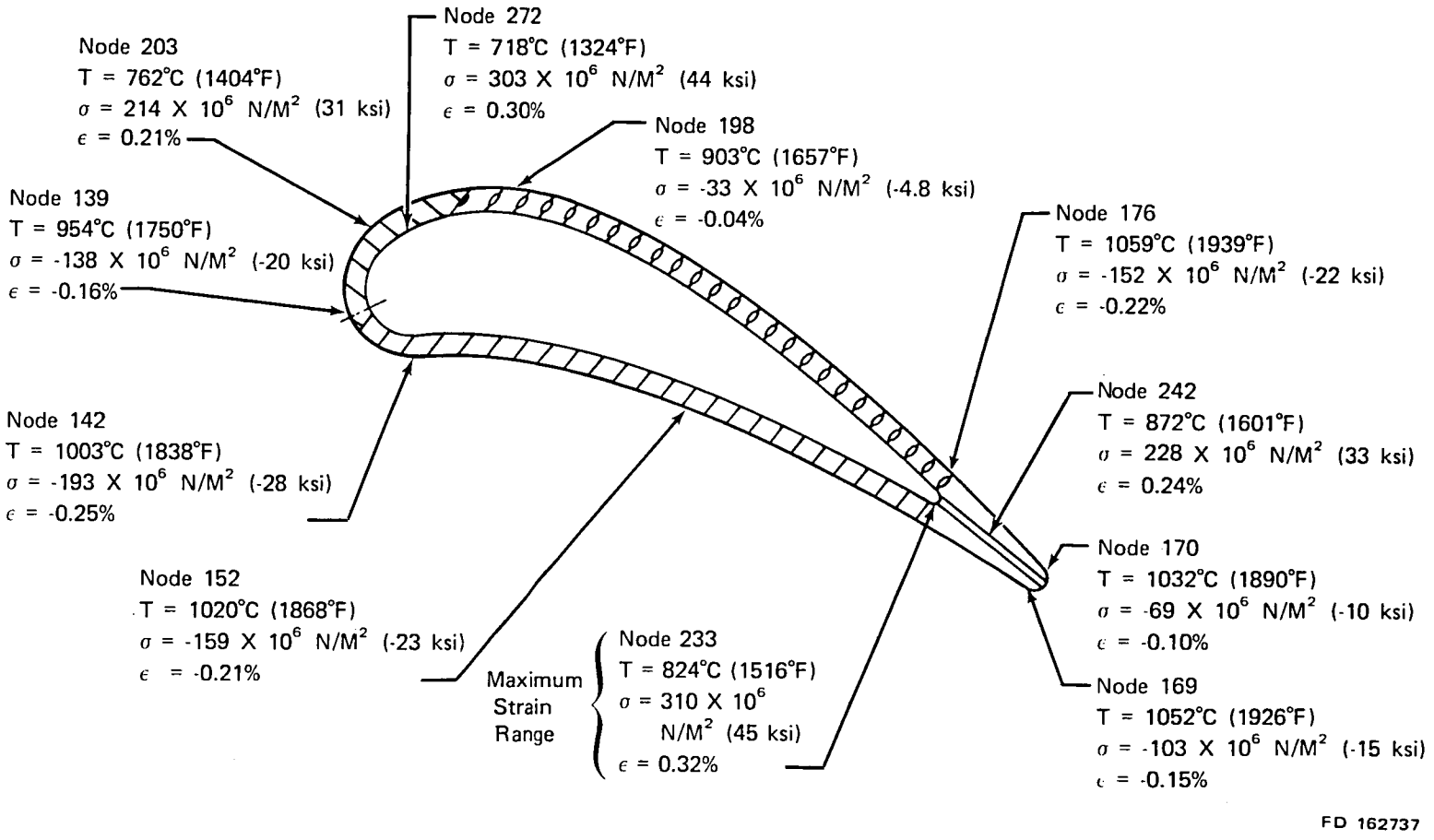

Figure 21. NASA Wafer Vane Design Point Local Stress/Strain Distribution

4. Oxidation/Erosion Life

The oxidation/erosion life evaluation was based on the bare Mar-M-200 + Hf material properties shown in figure 22. A design point life of 245 hr and an off-design point life of 78 hr were determined for the predicted hot spot metal temperature of 1060 and 1124°C (1940 and 2056°F). These predicted lives are sufficient to satisfy a typical cascade test program; however, for engine application a coating is recommended to prolong the airfoil life.

C. ENDWALL DESIGN RESULTS

The endwall cooling analysis was less detailed than that conducted for the vane, as explained previously in Section IV. For this area high coverage film cooling was utilized as the cooling scheme due to the severe gas environment conditions which were identical to the vane design conditions. Normally the endwall gas stream temperature is reduced from the vane hot spot temperature due to an inlet gas stream profile consisting of a hot temperature near midspan and cooler temperature at the endwalls. For the NASA cascade, however, the profile was defined as flat.

The cooling design geometry for the endwall is presented in figure 23. The total amount of coolant flowrate is 1.72% for each end-wall. The cooling scheme is a mixture of etched film holes and EDM film holes. The reason for the EDM holes is that in the areas where wafers were not required for the vane cooling a solid end block was used. Wafers could be used in these areas but for this program it was not necessary and endblocks were used to reduce the total number of parts and costs.

The endwall ISO-BAR distribution, shown in figure 24, was obtained through the use of the given endwall geometry and the inlet and exit conditions. Knowing the average static pressure distribution and streamline length, the external heat transfer coefficients were calculated using the turbulent flat plate correlation. This calculated value was adjusted based on the endwall experimental investigation results obtained from tests conducted within P&WA. The endwall nodal breakup, external heat transfer coefficients, and the hand calculated one-dimensional steady-state temperature distributions for the design and off-design points are presented in figures 25 and 26, respectively. The design point maximum metal temperature is 1070°C (1959°F). This temperature is approximately equal to the maximum metal temperature predicted for the vane surface. Since no durability analysis was conducted on the endwall, the life characteristics were not defined; however, the life is assumed approximately equal to that predicted with the vane since the maximum metal temperature is approximately the same.

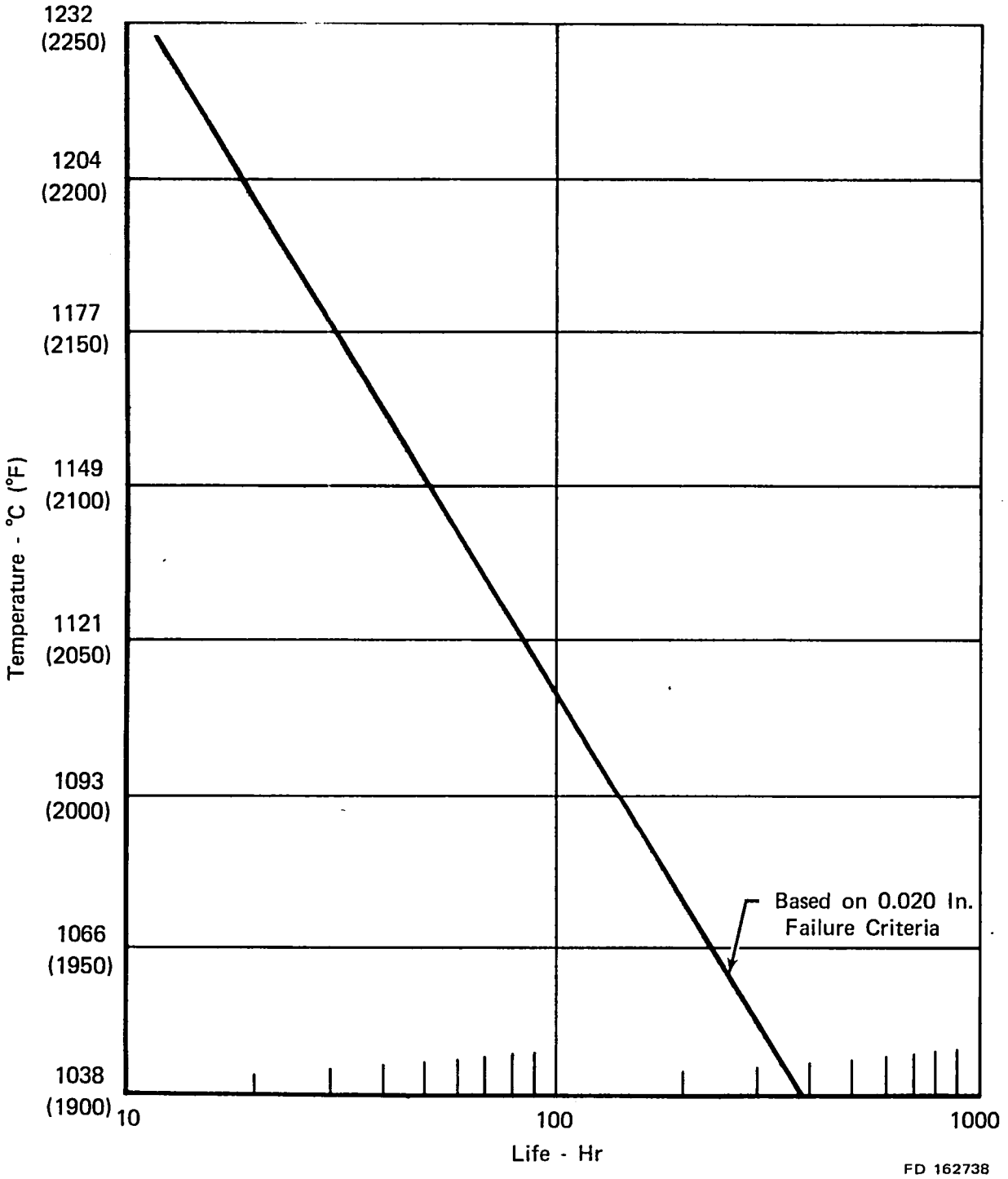

Figure 22. Oxidation/Erosion Life Prediction for PWA 1422

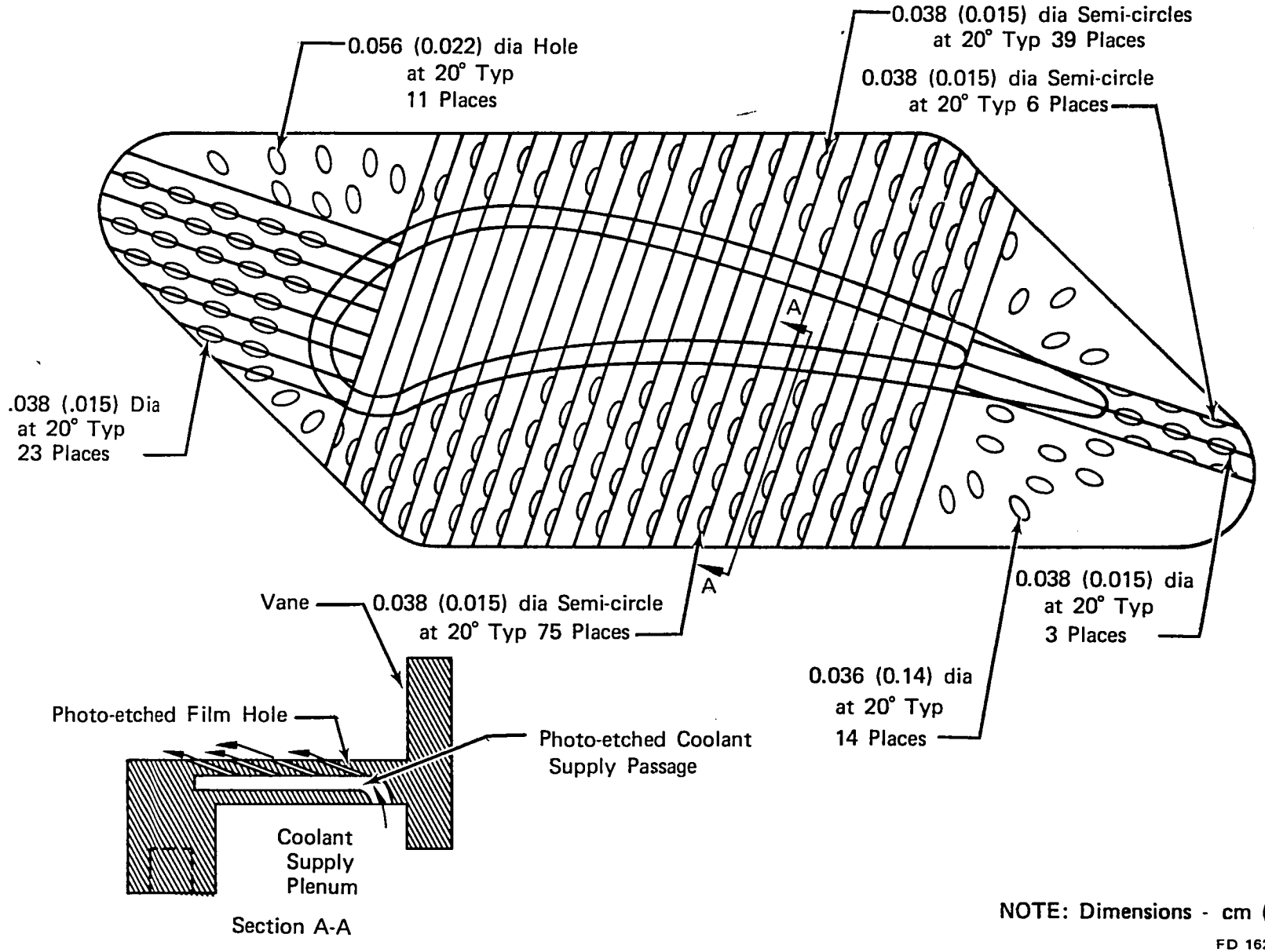

Figure 23. NASA Wafer Vane Endwall Cooling Geometry

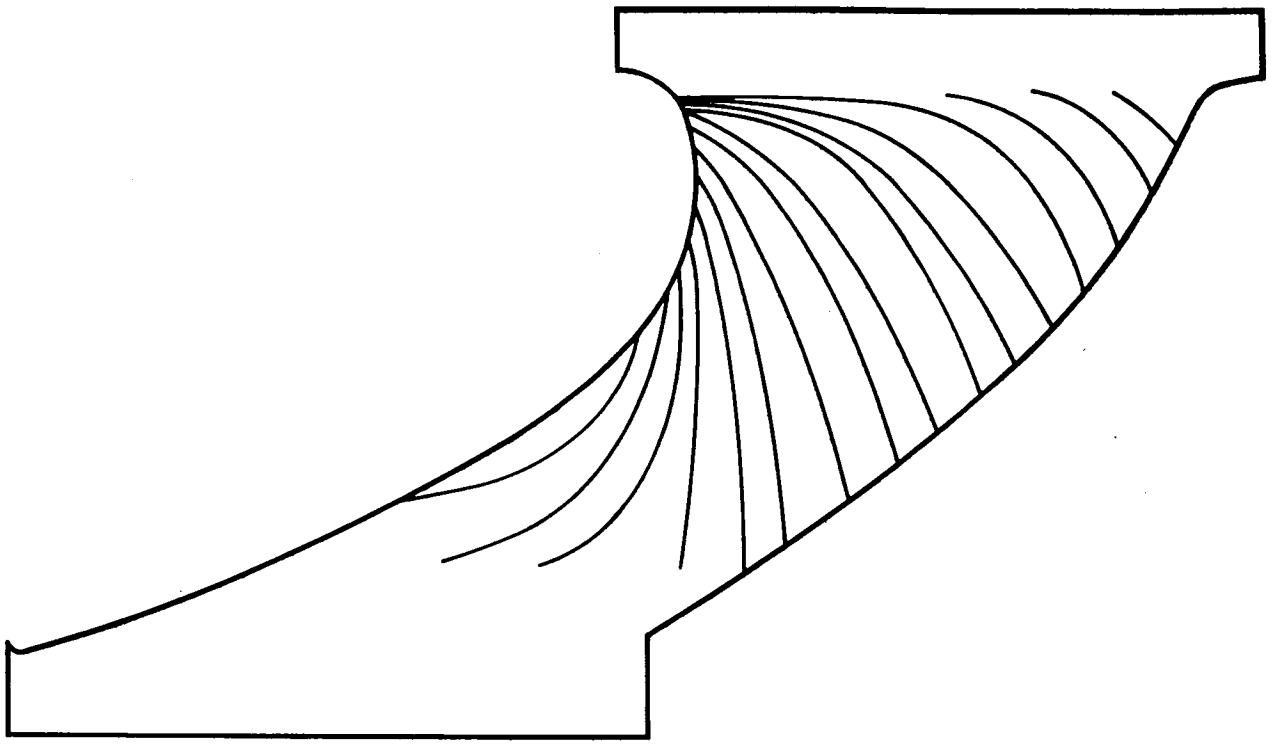

FD 162740

Figure 24. Endwall Iso-bar Line

Node	X′ - Distance		$T_{surface}$		h_g	
					Btu / Hr Ft^2 °F	Watt / M^2 °K
	(in.)	(cm)	(°F)	(°C)		
1	0.08	0.20	1959	1070	1253	7110
2	0.29	0.74	1930	1054	1216	6900
3	0.54	1.37	1914	1045	1272	7218
4	0.76	1.93	1871	1022	1284	7286
5	1.04	2.64	1865	1018	1293	7337
6	1.34	3.40	1904	1040	1298	7366
7	1.75	4.45	1948	1064	1270	7207
8	2.18	5.54	1878	1025	1256	7127
9	2.52	6.40	1896	1035	1298	7366
10			1891	1033	1450	8228
11			1728	942	1400	7944
12			1926	1052	1380	7831
13			1880	1027	1360	7717
14			1903	1039	1350	7661
15			1944	1062	1340	7604
16			1803	984	1320	7490
17			1702	928	1300	7377
18			1856	1013	1300	7377
19			1850	1010	1460	8285
20			1949	1065	1620	9193
21			1750	954	1320	7490
22			1672	911	1100	6242
23			1642	894	1180	6696
24			1673	912	1240	7036
25			1873	1023	1300	7377
26			1825	996	1320	7490
27			1760	960	1620	9193

Tg = 1538°C (2800°F)
Tc = 649°C (1200°F)
Pg = 4.136 X 10^6 N/M^2 (600 psia)
C/A = 1.72%

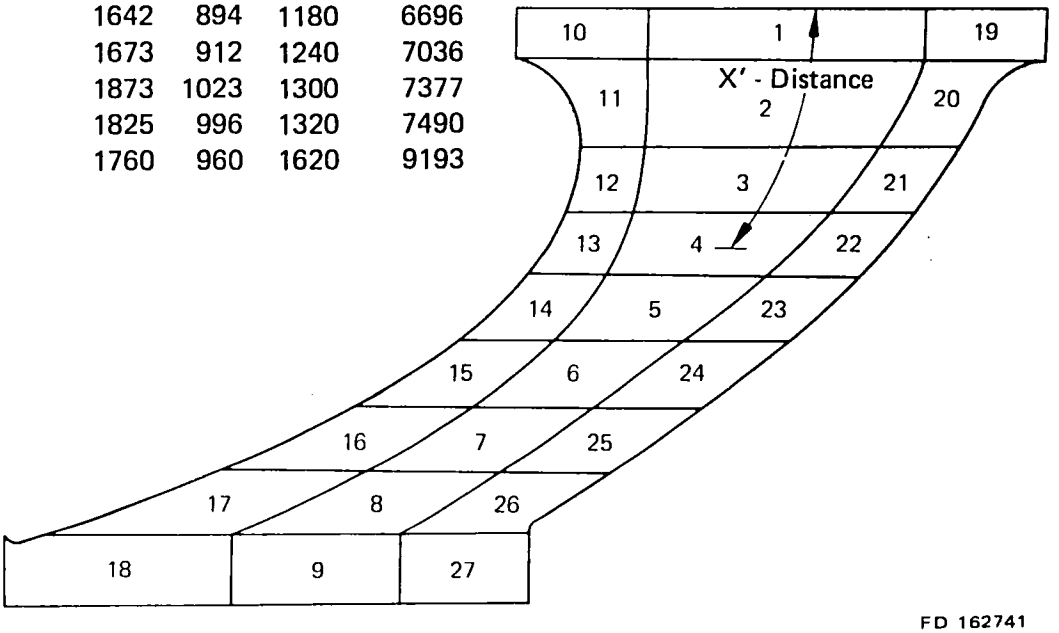

FD 162741

Figure 25. Endwall Steady State Temperature Distribution for Design Point

Node	X′ - Distance		$T_{surface}$		hg	
					Btu / Hr Ft^2 °F	Watt / M^2 °K
	(in.)	(cm)	(°F)	(°C)		
1	0.08	0.20	2027	1108	888	5039
2	0.29	0.74	2000	1093	860	4880
3	0.54	1.34	1969	1076	896	5084
4	0.76	1.93	1901	1038	901	5113
5	1.04	2.64	1903	1039	905	5135
6	1.34	3.40	1945	1063	907	5147
7	1.75	4.45	2006	1097	887	5033
8	2.18	5.54	1925	1052	877	4977
9	2.52	6.40	1947	1064	905	5135
10			2016	1102	1110	6299
11			1836	1002	1100	6242
12			2039	1115	1055	5987
13			1999	1093	1035	5873
14			2024	1107	1015	5760
15			2060	1127	995	5646
16			1864	1018	975	5533
17			1708	931	940	5334
18			1901	1038	940	5334
19			2041	1116	1200	6809
20			2167	1186	1330	7547
21			1860	1016	1060	6015
22			1881	1027	785	4454
23			1657	903	840	4767
24			1688	920	900	5107
25			1929	1054	930	5277
26			1863	1017	945	5362
27			1881	1027	1330	7547

Tg = 1927°C (3500°F)
Tc = 538°C (1000°F)
Pg = 2.758 X 10^6 N/M^2 (400 psia)
C/A = 1.68%

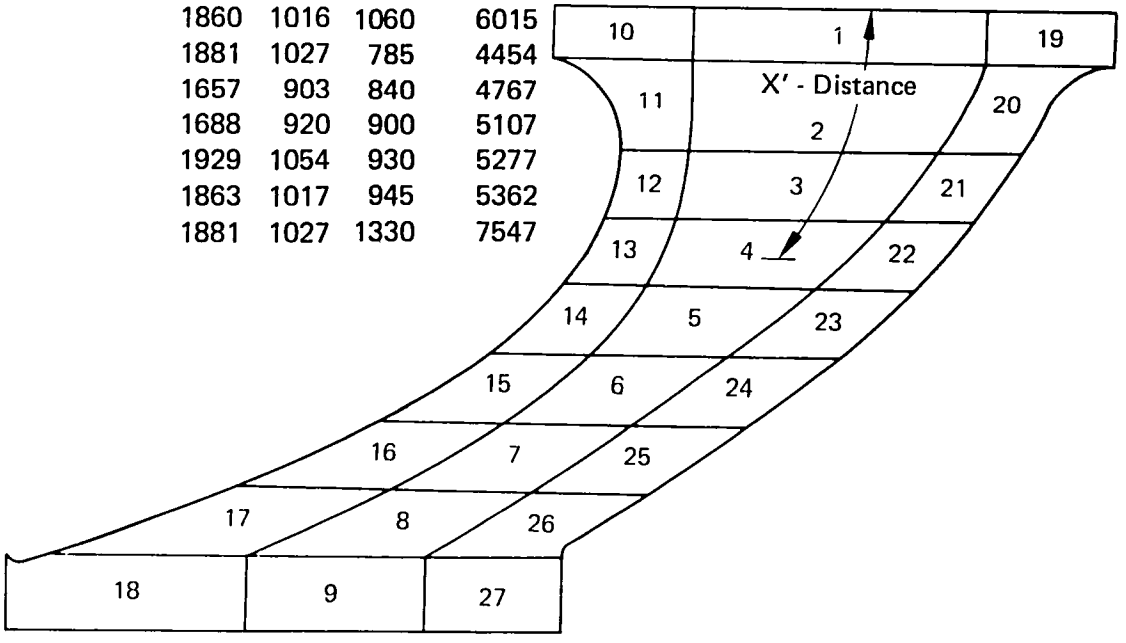

FD 162742

Figure 26. Endwall Steady State Temperature Distribution for Off-Design Point

VI. FABRICATION DESCRIPTION

The cooling design was incorporated into two cascade test vanes and associated endwalls using the radial wafer fabrication technique. The vanes are a constant cross-section design with a 3.81 cm (1.500 in.) span height. The wafers were etched utilizing an electrochemical process. The etching process was developed satisfactorily at P&WA/GPD Materials Laboratory; however, during the sample wafer etching work at the selected etching vendor facility, certain deviations were observed. The etching results were not acceptable due to resist coating (protective layer which prohibits etching) breakdown and excessive groove width and depth variation as indicated in figures 27 and 28.

The coating breakdown results in excessive pitting around the coolant passages. In wafer airfoil construction this may result in passages being exposed to the mainstream in regions not desired after the final machining operation. The excessive groove width and depth variation is not acceptable since an accurate definition of flow distribution in varying passages is impractical.

The etching system parameters between the laboratory and the vendor were checked for deviations and two parameters, electrolyte temperature and resist coating application, were found to vary. A study was conducted in the P&WA/GPD laboratory varying the electrolyte temperature between 7 and 41°C (45 and 106°F). Figure 29 presents the results of the study, indicating the cooler the electrolyte solution the better the etched groove definition. Therefore, an ice cooled bath to control electrolyte solution temperature was installed at the vendor. The method of applying the resist coating was switched from dipping the wafers in liquid to a thin-film form. The thin-film form of resist application was obtained by passing the wafer between two rollers that deposited a thin sheet of the resist material on each side of the wafer. This thin-film form of application resulted in an even resist coating and satisfactory etching results.

The vane airfoil and associated endwalls cooling scheme was fabricated utilizing thirty-three wafers and four endblocks. The wafer and endblock orientation is shown in figure 30. The wafers and endblocks that formed the leading edge showerhead and the trailing edge wavy crisscross slot were fabricated first. These were bonded into subassemblies and machined before being bonded with the remaining wafers to form the complete assemblies from which the cascade vanes were machined. The wafers and end blocks that form the leading edge and trailing subassemblies for one of the cascade vanes are shown in figures 31 and 32, respectively. The wafers which made up the main body of the vane, in addition to the leading and trailing edge bonded subassemblies, are shown in figure 33. One of the complete bonded block assemblies is shown in figure 34.

During the first bond cycle for the complete assembly, the load became misaligned and a slight fanning of the wafers was observed on the suction side. This produced some unbonded areas which were not removed during the final machining operation. Before initiating the second bond cycle, the bonding fixture was modified to eliminate the misalignment problem observed with the first block. The fixture modification was successful, as the second bonded block did not exhibit the fanning phenomenon observed with the first block. The completed cascade vane was obtained by electrical discharge machining the internal cavities and external contour.

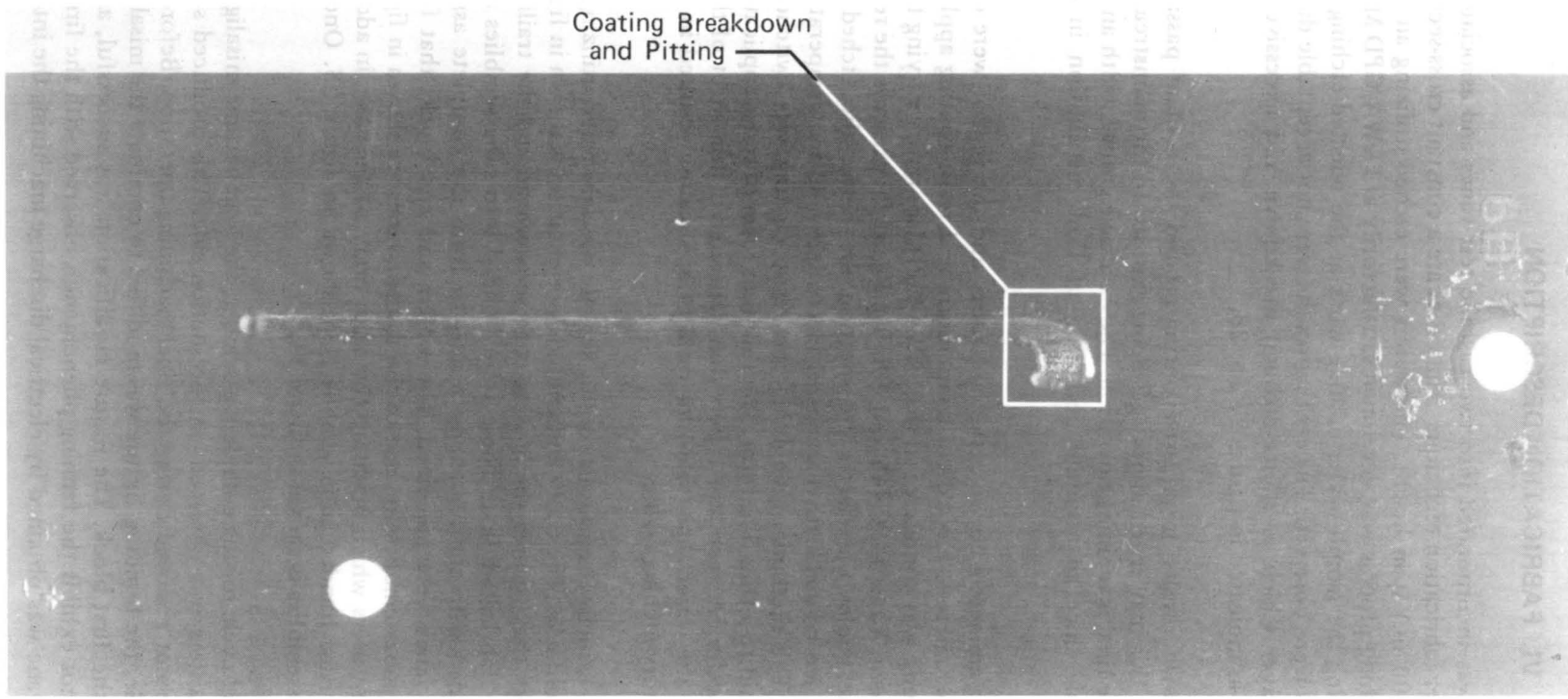

FE 164415 A

Figure 27. Etched Midchord Wafer Showing Resist Coating Breakdown and Passage Taper

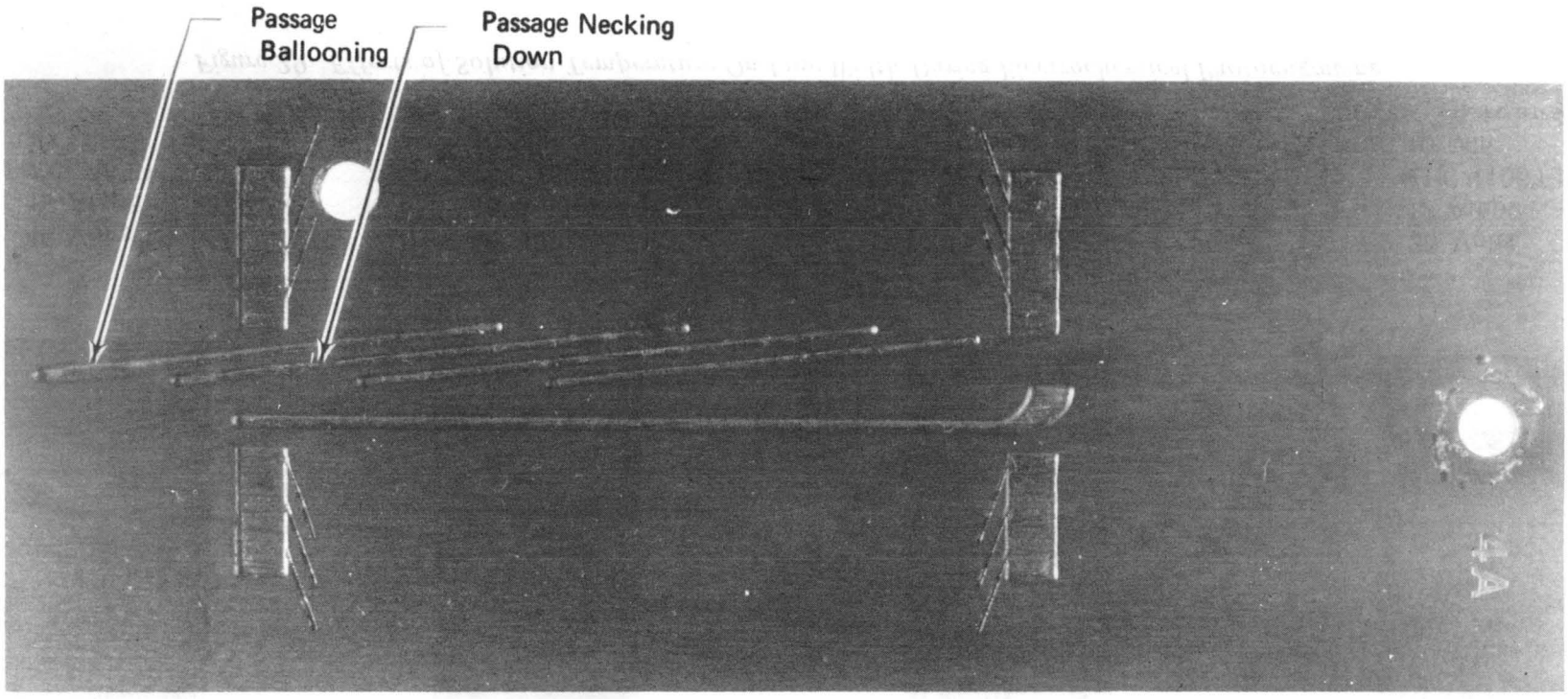

FE 164416 A

Figure 28. Etched Midchord Wafer Showing Passage Size Variation

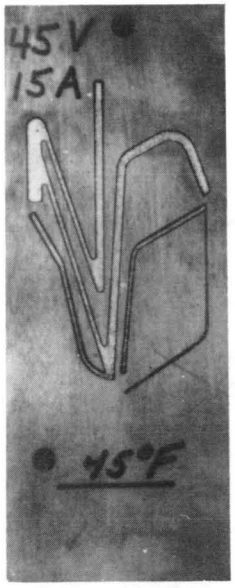

45 Volts
15 Amps
7°C (45°F)
10 Min

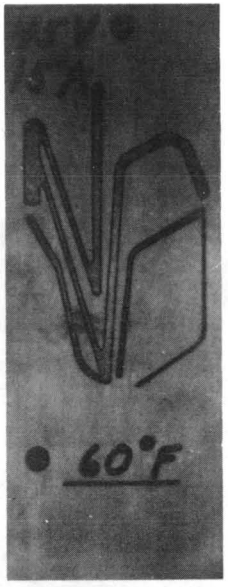

45 Volts
15 Amps
16°C (60°F)
10 Min

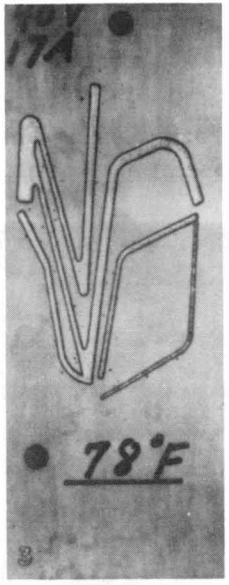

40 Volts
17 Amps
26°C (78°F)
10 Min

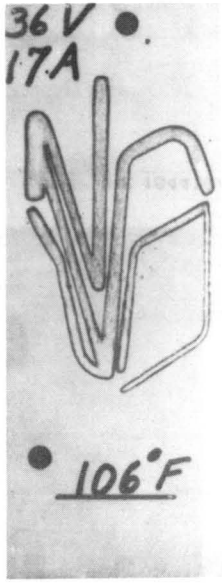

36 Volts
17 Amps
41°C (106°F)
10 Min

FC 37586 A

Figure 29. Effects of Solution Temperature On Line Width During Electrochemical Photoengraving

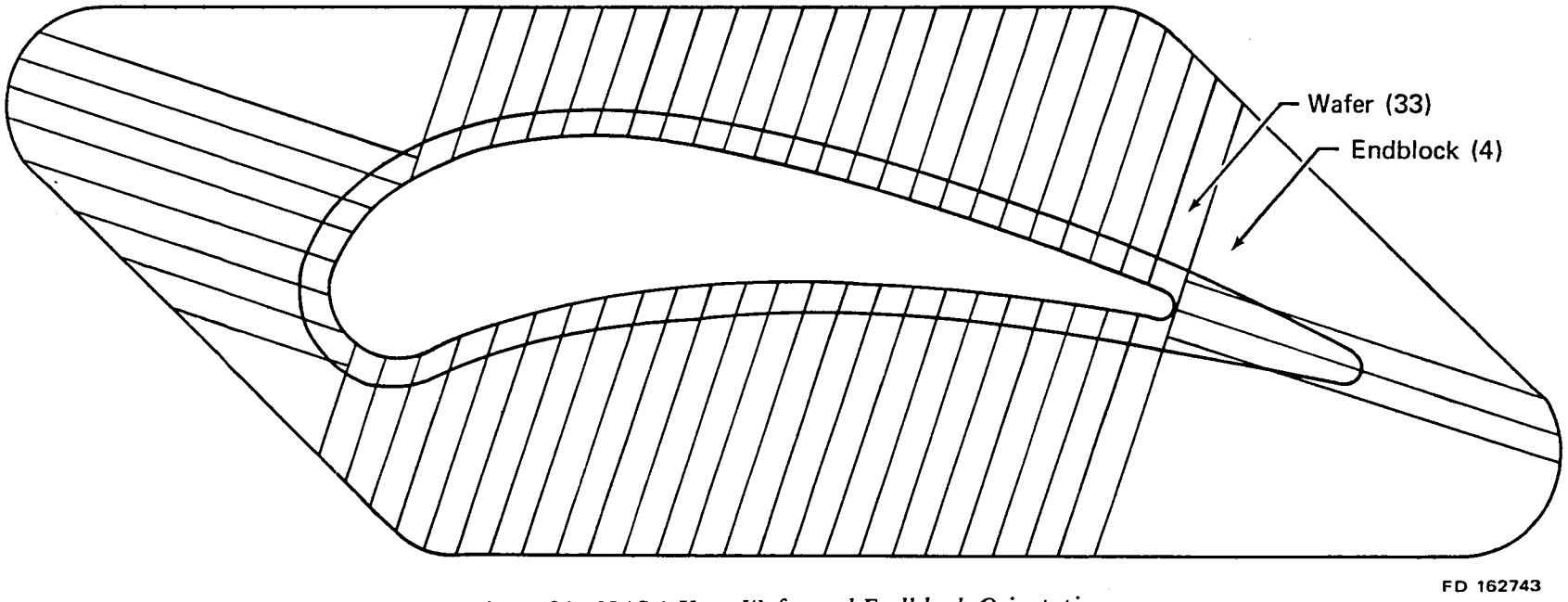

Figure 30. NASA Vane Wafer and Endblock Orientation

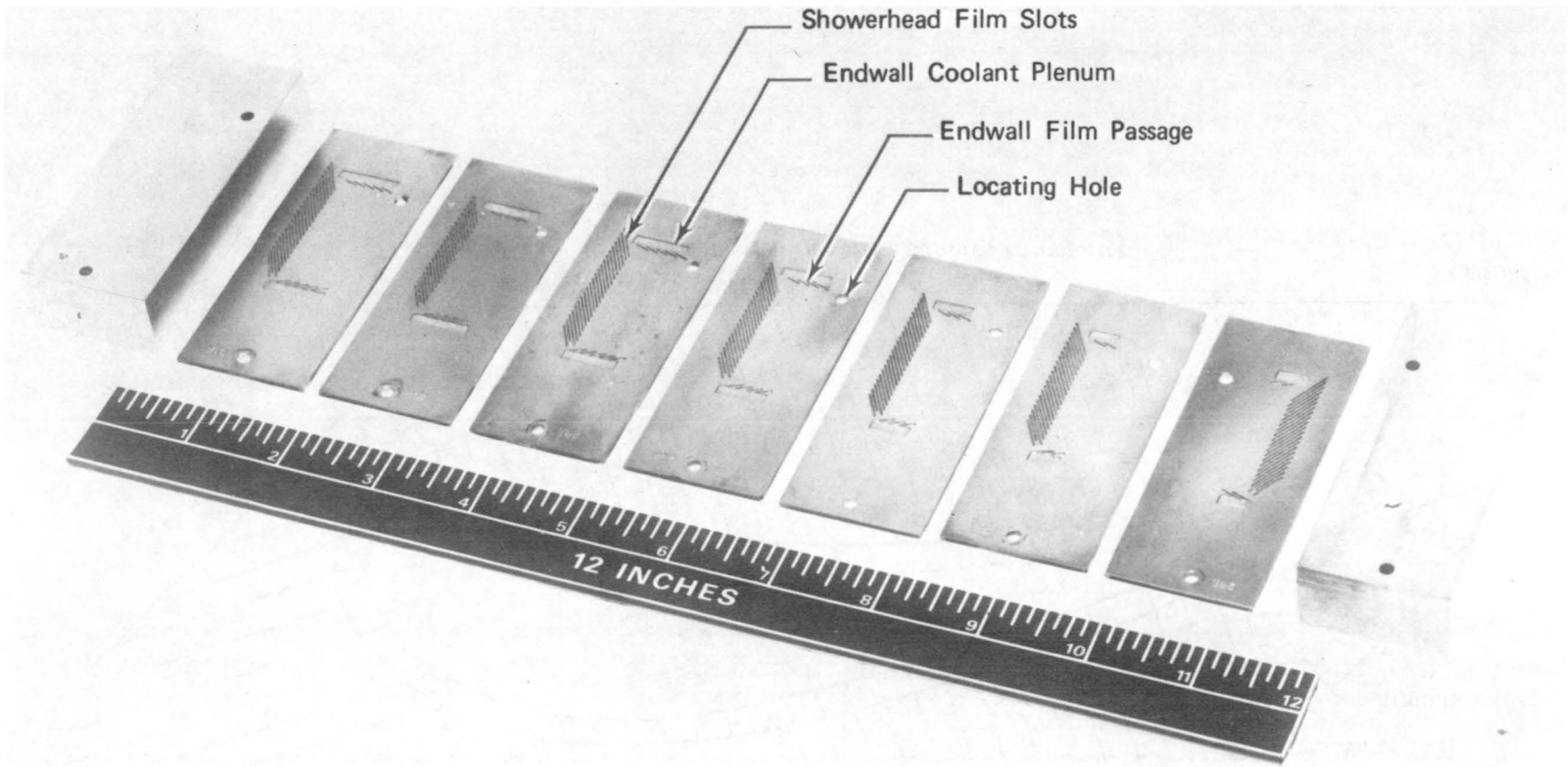

Figure 31. Etched Wafers and Blocks for NASA Wafer Vane Leading Edge Section

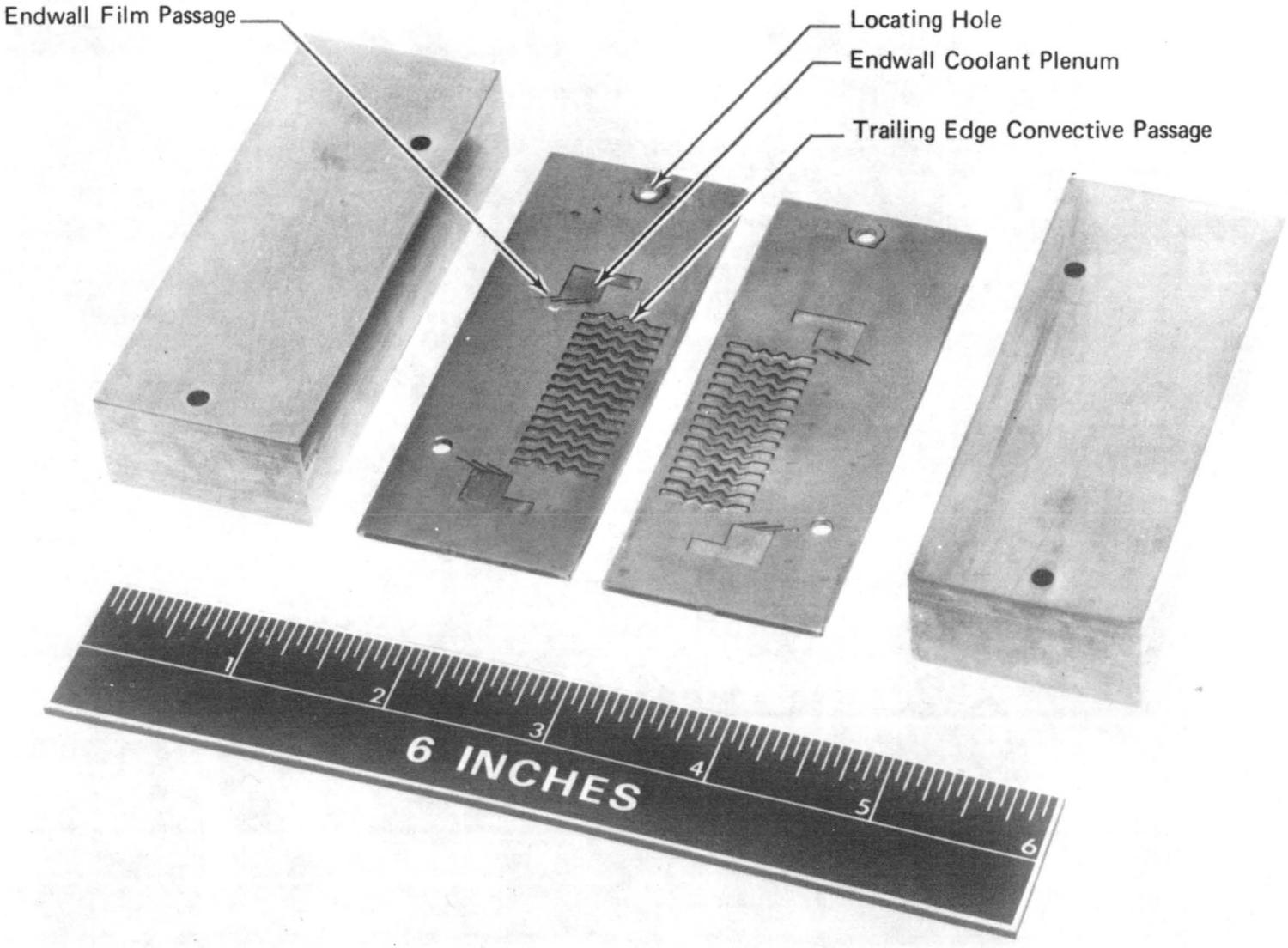

FAE 163566A

Figure 32. Etched Wafers and Blocks for NASA Wafer Vane Trailing Edge Section

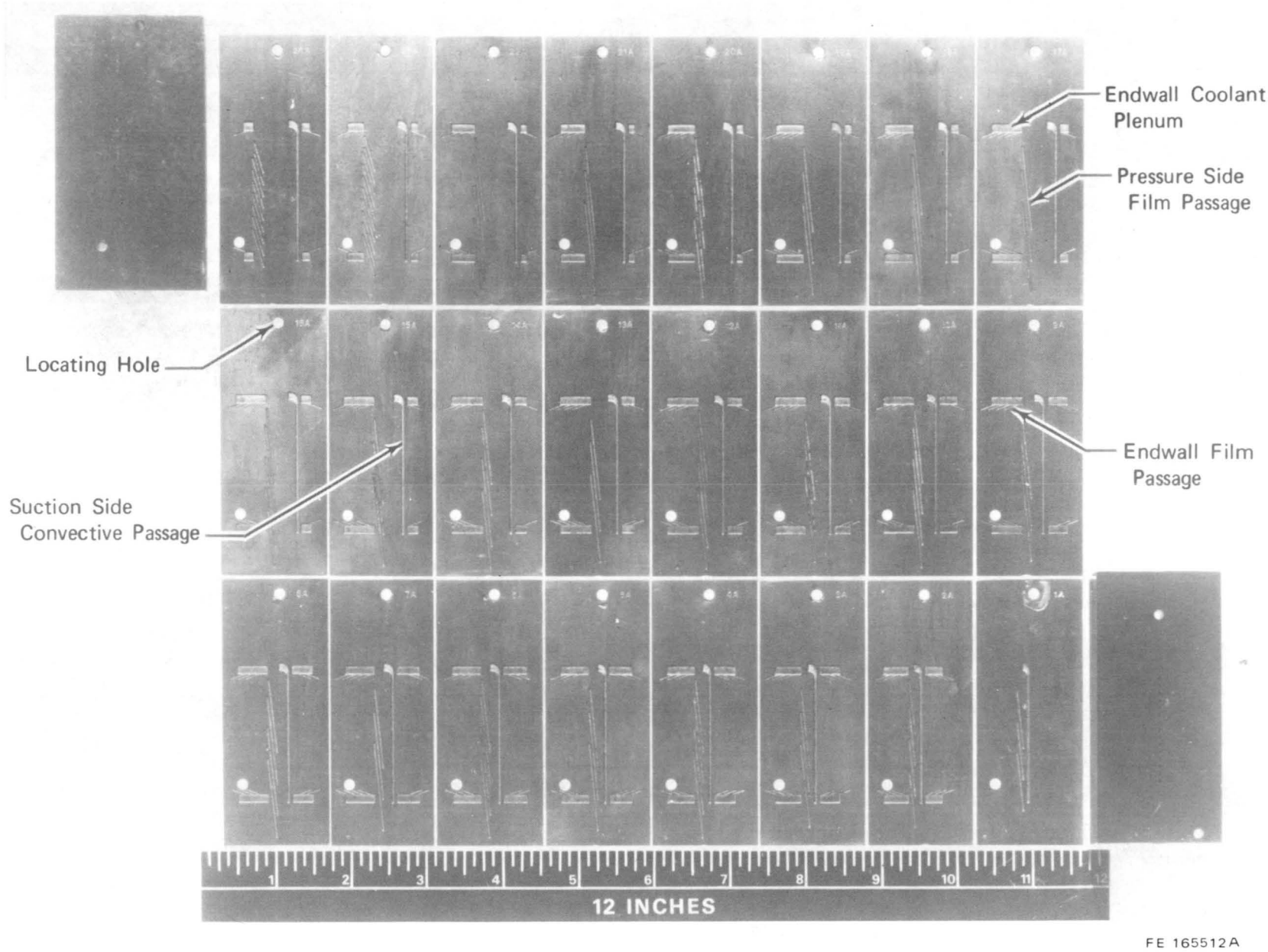

Figure 33. Leading Edge Block, Trailing Edge Block and Midchord Wafers for NASA Wafer Vane

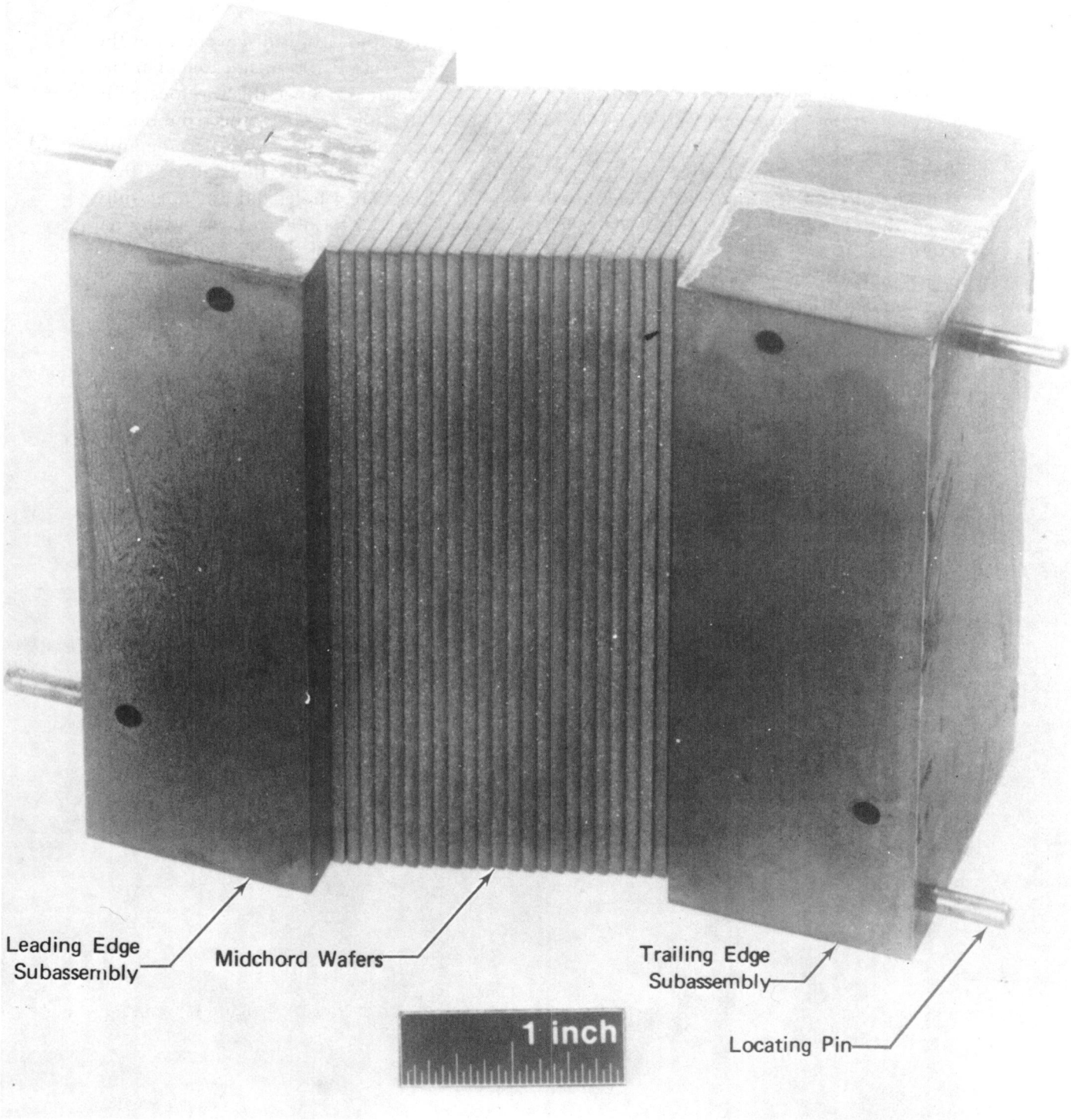

FAE 172468A

Figure 34. NASA Wafer Vane Bonded Assembly

During final machining of the suction side external contour, it was discovered that the etching pattern for the first wafer aft of the leading edge section was mislocated. This resulted in a slot running the full span length as shown in figure 35. Since this was located in a cool portion of the vane and was only one-half a passage, the result of the reduction in cooling air was assumed insignificant. In addition, since one of the four thermocouple slots was originally planned near that position, it was decided to utilize the slot for a thermocouple location. In addition, some of the endwall film cooling holes did not open fully when the airfoil was EDM'ed to the specified span of 3.81 cm (1.500 in.). An additional 0.076 cm (0.030 in.) is required to open these holes. The 3.81 cm (1.500 in.) span was retained since the additional EDM work could be done at a later date if fully opened film cooling holes are required.

The final steps in the fabrication process were the machining of the showerhead and platform film cooling holes and the thermocouple instrumentation slots. The two completed vanes and associated endwalls are shown in figure 36. Figure 37 shows the external contour inspection results of the second vane which is similar to that obtained with the first vane, indicating good agreement with the vane engineering drawing. A maximum of 0.013 and 0.015 cm (0.005 and 0.006 in.) oversize was obtained on the pressure side of the vane near the leading edge and on the platform near midchord, respectively.

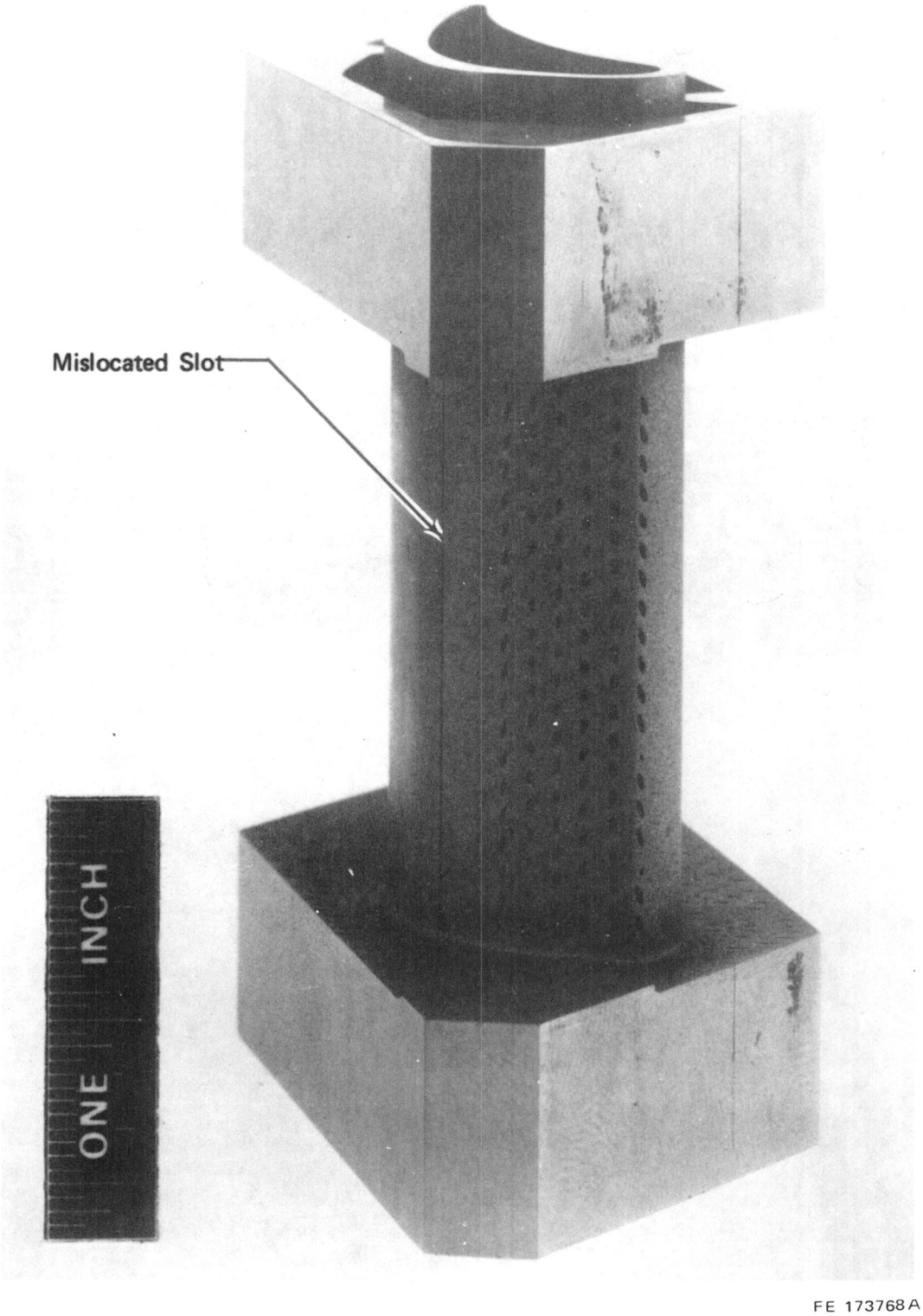

Figure 35. NASA Wafer Vane Showing Mislocated Suction Side Slot

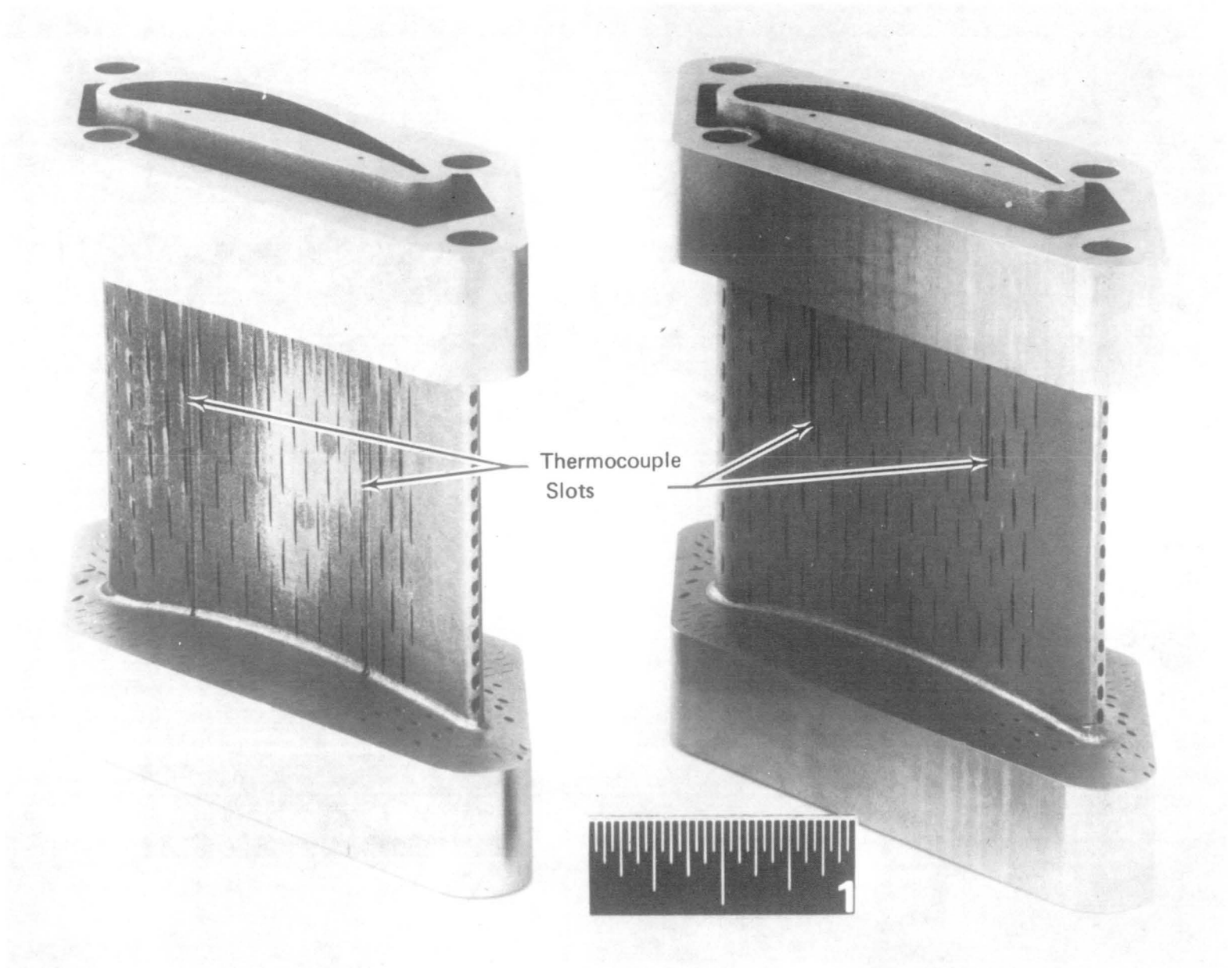

FE 176134A

Figure 36. NASA Wafer Vanes and Associated Endwalls

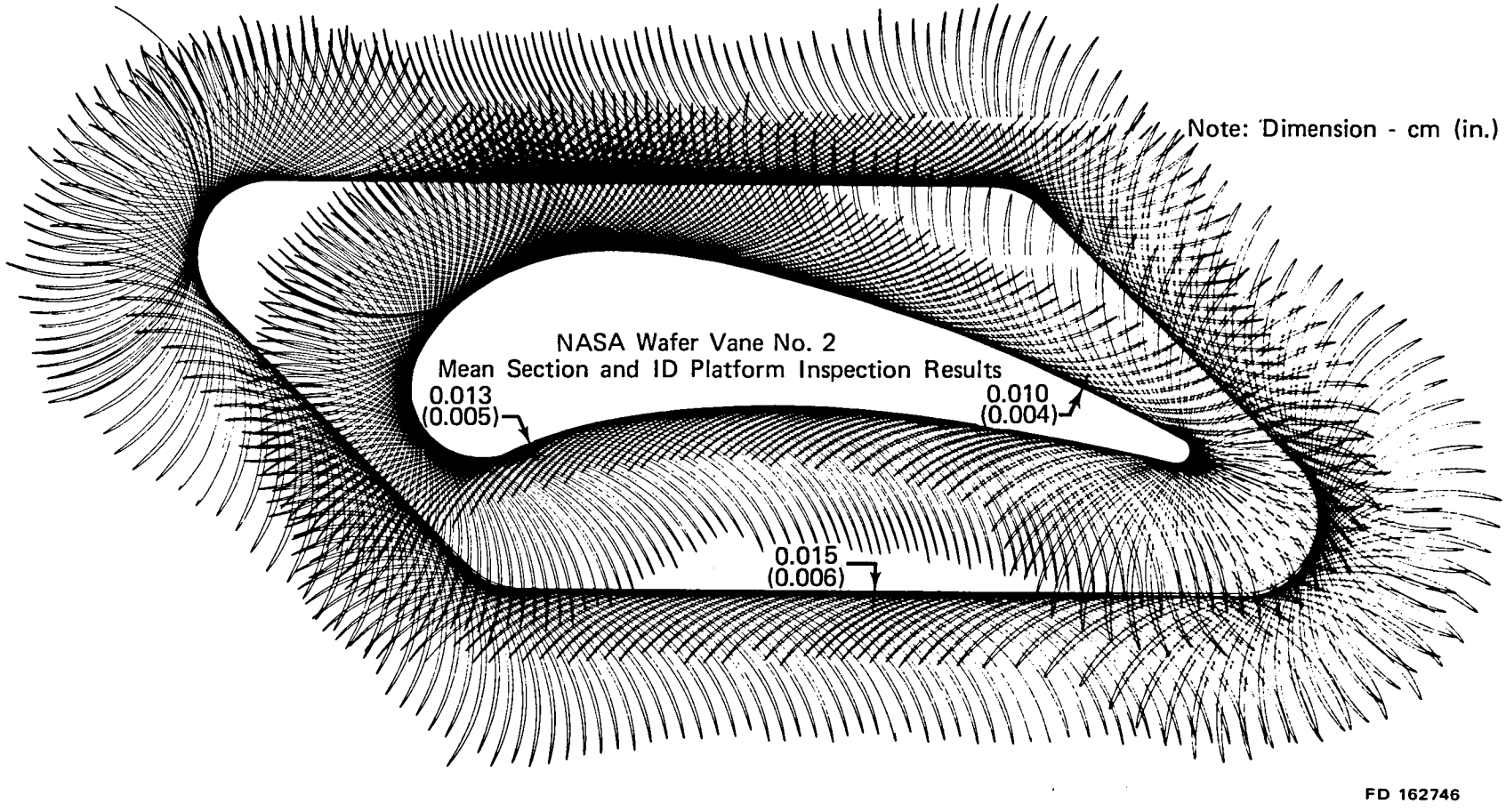

Figure 37. Radial Wafer Vane External Contour Inspection Results

VII. COLD FLOW CALIBRATION

A cold flow program was conducted with the two vanes upon completion of the fabrication process. The experimental results for the two vane airfoils along with the predicted curve are shown in figure 38 indicating good agreement. Endwall data are shown in figure 39 along with the predicted curve, and poor agreement was obtained. One reason contributing to the underflowing situation is that some of the coolant passages on the platform did not open up during the final machining operation. However, the number of passages not opening up was not sufficient to account for all of the discrepancy. Another probable source of error in the cold flow data was in measurement of coolant supply pressure. This parameter was measured outside of the platform cavity, and if a pressure drop exists between the location of measurement and the platform cavity, this would result in an indicated underflowing condition. The problem may have existed because in the endwall region a different supply manifold arrangement was used than with the airfoil. This arrangement was required to seal off airflow to the airfoil and only supply airflow to the platform cavity. In doing this a restriction may have been introduced between the platform cavity and the section where the coolant supply pressure was measured. Since measurement of this orifice area (if it did exist) was not practical, a correction could not be determined. It is recommended that once the coolant supply tubes are connected to the platform, this section be rechecked to determine if during actual cascade testing the supply pressure must be increased to obtain the design flowrate. A tabulation of the cold flow data and pressure ratio for the vanes and endwalls is included in Appendix A.

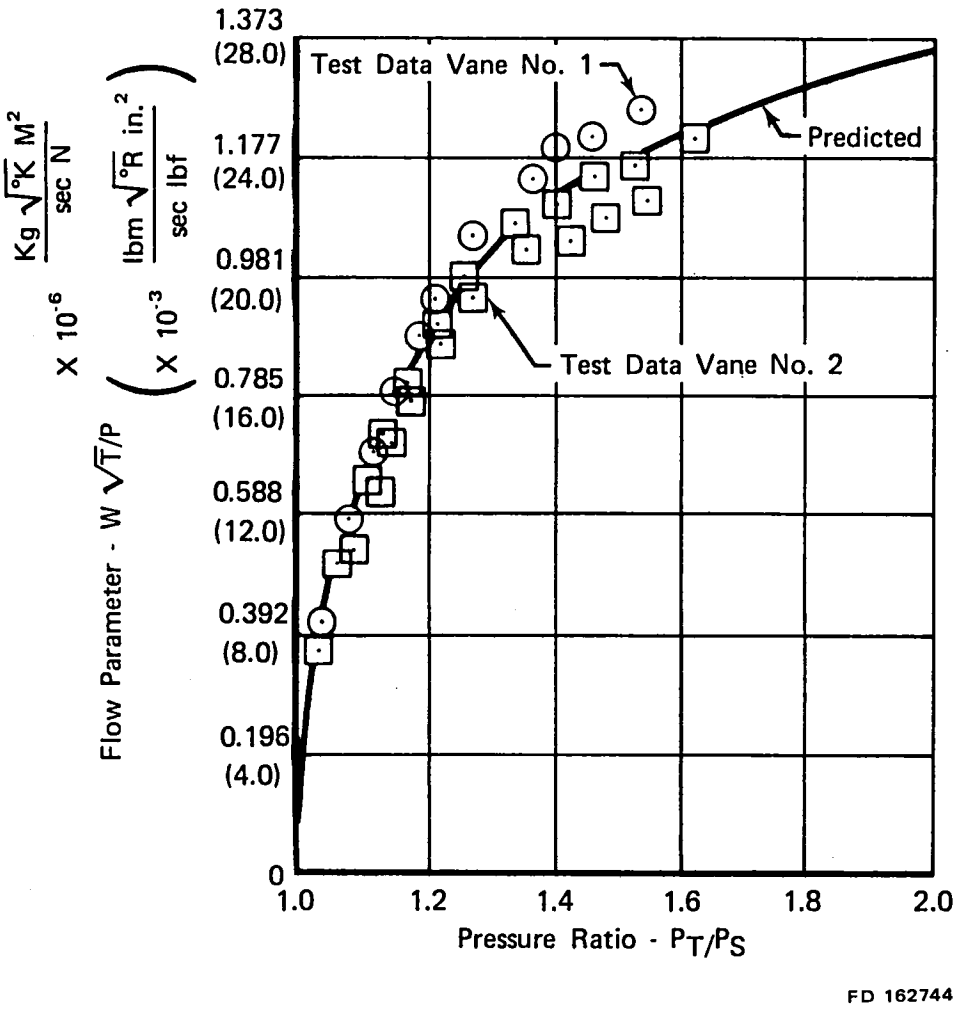

Figure 38. Cold Flow for NASA Radial Wafer Vane

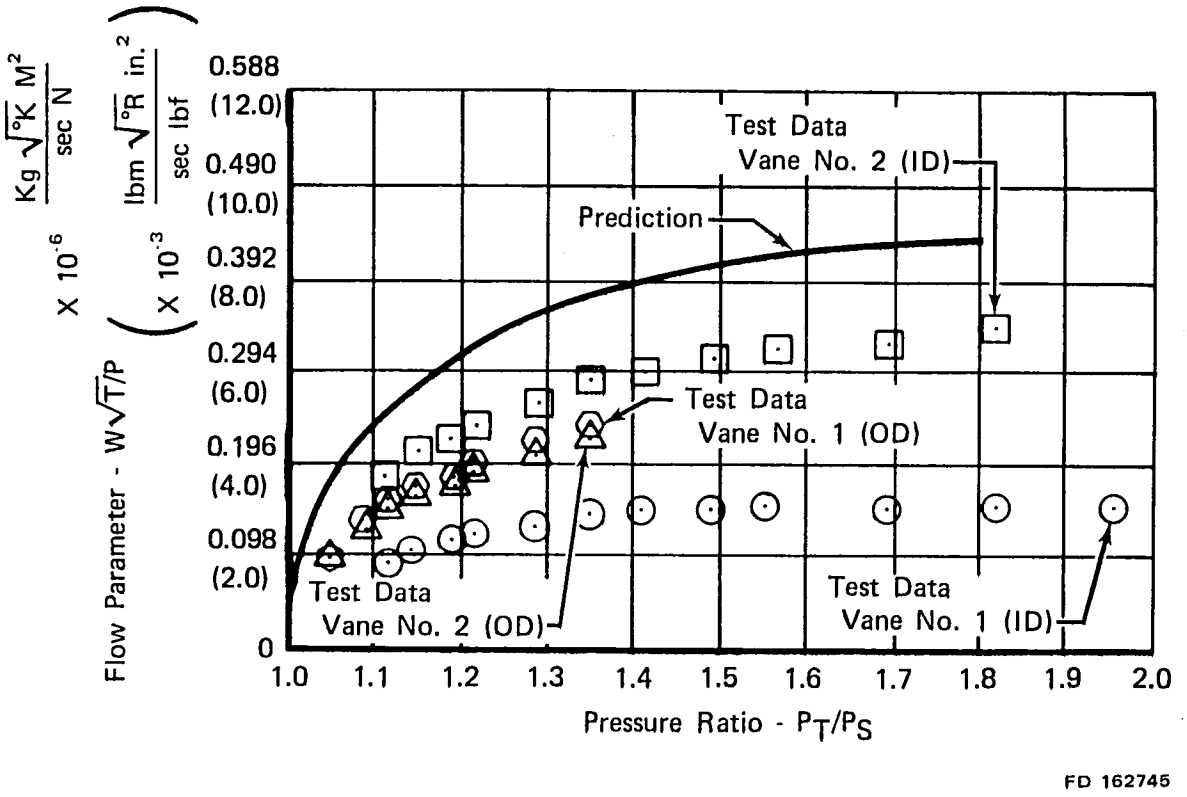

Figure 39. Cold Flow for NASA Radial Wafer Vane Endwall

VIII. CONCLUSIONS AND RECOMMENDATIONS

A. CONCLUSIONS

1. Use of an efficient convective cooling scheme on the suction side and in the trailing edge region of the NASA vane eliminated the need for film cooling in those regions and minimized the amount of convective coolant required.

2. Elimination of film cooling on the suction side will result in a vane design that is more desirable from an aerodynamic performance standpoint than one with film cooling on the suction side.

3. The effective cooling scheme was possible through the use of the radial wafer fabrication techniques which permit designs with small intricate connective passages not attainable in cast and drilled airfoils.

4. Use of the radial wafer fabricaton method permitted full coverage film cooling in the areas desired and allowed incorporation of the endwall cooling design into the wafers that formed the vane.

B. RECOMMENDATIONS

The cold flow calibration test for the endwalls should be repeated before conducting the hot cascade tests.

IX. APPENDIX A – REQUIRED DATA

Table 1. Pressure Side Chordwise Metal Temperatures for Design and Off-Design Points

			Temperature			
	Distance		Design Point		Off-Design Point	
Node	(in.)	(cm)	^oF	^oC	^oF	^oC
139	0.00	0.00	1750	954	1843	1006
140	0.10	0.25	1876	1024	2001	1094
141	0.18	0.46	1846	1008	1973	1078
142	0.26	0.66	1838	1003	1946	1063
143	0.33	0.84	1851	1011	1963	1073
144	0.40	1.02	1838	1003	1951	1066
145	0.47	1.19	1850	1010	1974	1079
146	0.54	1.37	1845	1007	1969	1076
147	0.61	1.55	1849	1009	1967	1075
148	0.68	1.73	1849	1009	1969	1076
149	0.75	1.91	1866	1019	1980	1082
150	0.82	2.08	1863	1017	1981	1083
151	0.89	2.26	1866	1019	1990	1088
152	0.96	2.44	1868	1020	1992	1089
153	1.03	2.62	1873	1023	2000	1093
154	1.11	2.82	1866	1019	1996	1091
155	1.18	3.00	1873	1023	1993	1089
156	1.25	3.18	1864	1018	1987	1086
157	1.32	3.35	1864	1018	1979	1082
158	1.39	3.53	1853	1012	1970	1077
159	1.46	3.71	1843	1006	1942	1061
160	1.53	3.89	1793	978	1862	1017
161	1.60	4.06	1728	942	1802	983
162	1.67	4.24	1706	930	1772	967
163	1.74	4.42	1742	950	1814	990
164	1.80	4.57	1812	989	1884	1029
165	1.87	4.75	1860	1016	1936	1058
166	1.93	4.90	1893	1034	1980	1082
167	2.00	5.08	1912	1044	2010	1099
168	2.06	5.23	1913	1045	2018	1103
169	2.13	5.41	1926	1052	2036	1113

Table 2. Suction Side Chordwise Metal Temperatures for Design and Off-Design Points

Node	Distance (in.)	Distance (cm)	Temperature, Design Point, °F	Temperature, Design Point, °C	Temperature, Off-Design Point, °F	Temperature, Off-Design Point, °C
207	0.08	0.20	1721	938	1801	983
206	0.17	0.43	1618	881	1642	894
205	0.26	0.66	1497	814	1466	797
204	0.33	0.84	1419	771	1362	739
203	0.40	1.02	1403	762	1335	724
202	0.46	1.17	1435	779	1370	743
201	0.53	1.35	1543	839	1518	826
200	0.60	1.52	1576	858	1570	854
199	0.66	1.68	1613	878	1602	872
198	0.73	1.85	1656	902	1647	897
197	0.80	2.03	1699	926	1700	927
196	0.86	2.18	1745	952	1753	956
195	0.93	2.36	1781	972	1806	985
194	1.00	2.54	1812	989	1844	1007
193	1.06	2.69	1833	1000	1877	1025
192	1.13	2.87	1848	1009	1905	1041
191	1.19	3.02	1853	1012	1926	1052
190	1.26	3.20	1878	1026	1953	1067
189	1.33	3.38	1889	1032	1973	1078
188	1.39	3.53	1899	1037	1991	1088
187	1.46	3.71	1908	1042	2001	1044
186	1.52	3.86	1910	1043	2006	1097
185	1.59	4.04	1916	1048	2016	1102
184	1.66	4.22	1918	1048	2023	1106
183	1.72	4.37	1924	1051	2031	1110
182	1.79	4.55	1928	1053	2039	1115
181	1.86	4.72	1931	1055	2046	1119
180	1.92	4.88	1934	1057	2052	1122
179	1.99	5.05	1936	1058	2056	1124
178	2.06	5.23	1938	1059	2056	1124
177	2.12	5.38	1937	1058	2053	1123
176	2.19	5.56	1938	1059	2044	1118
175	2.54	6.45	1908	1042	1988	1087
174	2.32	5.89	1887	1031	1962	1072
173	2.39	6.07	1878	1026	1960	1071
172	2.45	6.23	1873	1023	1962	1072
171	2.52	6.40	1870	1021	1964	1073
170	2.58	6.55	1890	1032	1992	1089

Table 3. Design Point Temperatures

Node	Temperature °F	Node	Temperature °F	Node	Temperature °F	Node	Temperature °F
1	1786	51	1549	101	1857	151	1866
2	1861	52	1579	102	1859	152	1868
3	1786	53	1608	103	1447	153	1873
4	1798	54	1633	104	1397	154	1866
5	1788	55	1654	105	1550	155	1873
6	1795	56	1670	106	1486	156	1864
7	1790	57	1682	107	1651	157	1864
8	1807	58	1691	108	1579	158	1853
9	1798	59	1706	109	1664	159	1843
10	1802	60	1719	110	1579	160	1793
11	1796	61	1729	111	1793	161	1728
12	1805	62	1739	112	1708	162	1706
13	1793	63	1745	113	1786	163	1742
14	1803	64	1751	114	1719	164	1812
15	1789	65	1753	115	1829	165	1860
16	1794	66	1759	116	1668	166	1893
17	1775	67	1762	117	1595	167	1912
18	1767	68	1764	118	1739	168	1913
19	1705	69	1766	119	1812	169	1926
20	1657	70	1767	120	1657	170	1890
21	1632	71	1769	121	1633	171	1870
22	1676	72	1772	122	1785	172	1873
23	1729	73	1770	123	1811	173	1878
24	1746	74	1375	124	1672	174	1887
25	1728	75	1361	125	1676	175	1908
26	1739	76	1391	126	1821	176	1938
27	1727	77	1510	127	1815	177	1937
28	1737	78	1538	128	1695	178	1938
29	1727	79	1565	129	1714	179	1936
30	1743	80	1600	130	1846	180	1934
31	1729	81	1635	131	1820	181	1931
32	1734	82	1672	132	1718	182	1926
33	1720	83	1703	133	1747	183	1924
34	1732	84	1733	134	1860	184	1918
35	1716	85	1752	135	1831	185	1916
36	1729	86	1765	136	1741	186	1910
37	1711	87	1773	137	1765	187	1908
38	1719	88	1788	138	1865	188	1899
39	1694	89	1800	139	1750	189	1889
40	1688	90	1811	140	1876	190	1878
41	1617	91	1821	141	1846	191	1853
42	1583	92	1829	142	1838	192	1848
43	1557	93	1835	143	1851	193	1833
44	1601	94	1838	144	1838	194	1812
45	1335	95	1843	145	1850	195	1781
46	1324	96	1847	146	1845	196	1745
47	1353	97	1849	147	1849	197	1699
48	1474	98	1852	148	1849	198	1656
49	1500	99	1854	149	1866	199	1613
50	1521	100	1855	150	1863	200	1576

Table 3. Design Point Temperatures (Continued)

Node	Temperature ^{o}F	Node	Temperature ^{o}F	Node	Temperature ^{o}F	Node	Temperature ^{o}F
201	1543	220	1734	239	1673	258	1710
202	1435	221	1720	240	1665	259	1698
203	1403	222	1732	241	1632	260	1683
204	1419	223	1716	242	1661	261	1673
205	1497	224	1729	243	1574	262	1662
206	1618	225	1711	244	1573	263	1646
207	1721	226	1719	245	1763	264	1626
208	1579	227	1694	246	1764	265	1601
209	1708	228	1688	247	1761	266	1573
210	1719	229	1617	248	1759	267	1543
211	1729	230	1583	249	1757	268	1516
212	1746	231	1557	250	1756	269	1495
213	1728	232	1601	251	1754	270	1470
214	1739	233	1315	252	1751	271	1353
215	1727	234	1555	253	1747	272	1374
216	1737	235	1604	254	1743	273	1335
217	1727	236	1648	255	1737	274	1397
218	1743	237	1684	256	1736	275	1486
219	1729	238	1713	257	1721	276	1579

Table 4. Off-Design Point Temperatures

Node	Temperature ^{o}F	Node	Temperature ^{o}F	Node	Temperature ^{o}F	Node	Temperature ^{o}F
1	1892	51	1535	101	1965	151	1990
2	1910	52	1573	102	1956	152	1992
3	1896	53	1611	103	1404	153	2000
4	1916	54	1648	104	1341	154	1996
5	1907	55	1678	105	1560	155	1993
6	1911	56	1704	106	1481	156	1987
7	1905	57	1726	107	1715	157	1979
8	1918	58	1747	108	1626	158	1970
9	1910	59	1768	109	1742	159	1942
10	1921	60	1788	110	1639	160	1869
11	1915	61	1805	111	1907	161	1802
12	1926	62	1818	112	1810	162	1772
13	1915	63	1828	113	1905	163	1814
14	1919	64	1838	114	1827	164	1884
15	1904	65	1846	115	1899	165	1936
16	1904	66	1853	116	1711	166	1980
17	1883	67	1859	117	1620	167	2010
18	1860	68	1864	118	1797	168	2018
19	1776	69	1867	119	1879	169	2036
20	1720	70	1870	120	1702	170	1992
21	1691	71	1871	121	1674	171	1964
22	1738	72	1870	122	1850	172	1962
23	1831	73	1855	123	1885	173	1960
24	1850	74	1303	124	1728	174	1962
25	1832	75	1278	125	1736	175	1988
26	1850	76	1315	126	1899	176	2044
27	1837	77	1477	127	1897	177	2053
28	1847	78	1522	128	1764	178	2056
29	1834	79	1551	129	1791	179	2056
30	1849	80	1589	130	1936	180	2052
31	1832	81	1634	131	1909	181	2046
32	1844	82	1679	132	1799	182	2039
33	1830	83	1723	133	1838	183	2031
34	1845	84	1762	134	1960	184	2023
35	1827	85	1792	135	1928	185	2016
36	1838	86	1817	136	1830	186	2006
37	1816	87	1838	137	1865	187	2001
38	1822	88	1858	138	1971	188	1991
39	1791	89	1878	139	1843	189	1973
40	1771	90	1895	140	2001	190	1953
41	1676	91	1908	141	1973	191	1926
42	1632	92	1919	142	1946	192	1905
43	1600	93	1929	143	1963	193	1877
44	1648	94	1937	144	1951	194	1844
45	1247	95	1945	145	1974	195	1806
46	1226	96	1952	146	1969	196	1753
47	1266	97	1958	147	1967	197	1700
48	1432	98	1962	148	1969	198	1647
49	1476	99	1966	149	1980	199	1602
50	1502	100	1966	150	1981	200	1570

Table 4. Off-Design Point Temperatures (Continued)

Node	Temperature °F	Node	Temperature °F	Node	Temperature °F	Node	Temperature °F
201	1518	220	1844	239	1757	258	1779
202	1370	221	1830	240	1742	259	1759
203	1335	222	1845	241	1695	260	1738
204	1362	223	1827	242	1649	261	1717
205	1466	224	1838	243	1608	262	1695
206	1642	225	1816	244	1596	263	1669
207	1801	226	1822	245	1847	264	1639
208	1639	227	1791	246	1861	265	1603
209	1810	228	1771	247	1862	266	1565
210	1827	229	1676	248	1861	267	1528
211	1831	230	1632	249	1858	268	1495
212	1850	231	1600	250	1854	269	1470
213	1832	232	1648	251	1850	270	1427
214	1850	233	1519	252	1844	271	1266
215	1837	234	1584	253	1837	272	1226
216	1847	235	1655	254	1828	273	1247
217	1834	236	1718	255	1819	274	1341
218	1849	237	1771	256	1809	275	1481
219	1852	238	1810	257	1796	276	1626

Table 5. Flowrate and Pressure Ratio for NASA Wafer Vane No. 1 at Ambient Conditions

Point	Pressure Ratio	Flowrate ($Kg/sec \times 10^{-4}$)	Flowrate ($lbm/sec \times 10^{-3}$)
1	1.03	23.46	5.17
2	1.07	36.14	7.97
3	1.10	44.93	9.91
4	1.14	53.14	11.72
5	1.17	59.60	13.14
6	1.20	66.45	14.65
7	1.27	78.22	17.24
8	1.34	88.71	19.56
9	1.40	98.29	21.67
10	1.47	104.49	23.12
11	1.54	113.34	24.99

Table 6. Flowrate and Pressure Ratio for NASA Wafer Vane No. 2 at Ambient Conditions

Point	Pressure Ratio	Flowrate ($Kg/sec \times 10^{-4}$)	Flowrate ($lbm/sec \times 10^{-3}$)
1	1.03	22.38	4.93
2	1.07	34.20	7.54
3	1.10	42.49	9.37
4	1.14	50.34	11.10
5	1.17	56.52	12.46
6	1.20	62.75	13.83
7	1.27	73.68	16.24
8	1.34	83.32	18.37
9	1.40	92.66	20.43
10	1.47	101.22	22.31
11	1.54	107.17	23.63
12	1.67	122.10	26.92

Table 7. Flowrate and Pressure Ratio for NASA Wafer Vane No. 1 Endwall at Ambient Conditions

		Flowrate			
		OD Endwall		ID Endwall	
Point	Pressure Ratio	(Kg/sec x 10^{-4})	(lbm/sec x 10^{-3})	(Kg/sec x 10^{-4})	(lbm/sec x 10^{-4})
1	1.05	5.99	1.32	–	–
2	1.08	8.20	1.81	–	–
3	1.12	9.78	2.16	6.06	1.34
4	1.15	11.38	2.51	6.94	1.53
5	1.18	12.54	2.76	7.62	1.68
6	1.22	13.92	3.07	8.34	1.84
7	1.28	16.19	3.57	9.58	2.11
8	1.35	18.37	4.05	10.60	2.34
9	1.42	–	–	11.54	2.54
10	1.49	–	–	12.35	2.72
11	1.55	–	–	13.14	2.89
12	1.67	–	–	14.43	3.18
13	1.82	–	–	15.63	3.45
14	1.96	–	–	16.56	3.65

Table 8. Flowrate and Pressure Ratio for NASA Wafer Vane No. 2 Endwall at Ambient Conditions

		Flowrate			
		OD Endwall		ID Endwall	
Point	Pressure Ratio	(Kg/sec x 10^{-4})	(lbm/sec x 10^{-3})	(Kg/sec x 10^{-4})	(lbm/sec x 10^{-4})
1	1.05	5.69	1.25	–	–
2	1.08	7.82	1.72	–	–
3	1.12	9.29	2.05	11.89	2.62
4	1.15	10.88	2.40	13.68	3.02
5	1.18	12.19	2.69	15.29	3.37
6	1.22	13.39	2.95	16.82	3.71
7	1.28	15.59	3.44	19.62	4.32
8	1.35	17.63	3.89	22.14	4.88
9	1.42	–	–	24.44	5.39
10	1.49	–	–	26.69	5.88
11	1.55	–	–	28.80	6.35
12	1.67	–	–	32.83	7.24
13	1.82	–	–	36.62	8.07

X. APPENDIX B
LIST OF SYMBOLS

Symbol *Definition*

English

C/A - Cooling Air
D_e - Equivalent Diameter
hg - External Heat Transfer Coefficient
L - Chord Length
L/E - Leading Edge
M - Blowing Parameter = $\frac{(\rho v)_{coolant}}{(\rho v)_{mainstream}}$
q/A - Heat Transfer Per Unit Area
P - Pressure
P_g - Mainstream Gas Pressure
P_S - Coolant Exit Static Pressure
P_T - Coolant Inlet Total Pressure
S - Film Slot Height
T - Temperature
T_c - Coolant Temperature
$T_{c,e}$ - Exit Coolant Temperature
T_f - Film Temperature
T_g - Mainstream Gas Temperature
T_m - Metal Temperature
V,v - Velocity
V_{CR} - Critical Velocity
W - Flowrate
X - Distance Along Absisa
X' - Surface Distance Along Endwall
x - Distance Downstream From Film Passage
Y - Distance Along Coordinate

Greek

ϵ - Strain
η - Film Effectiveness Parameter = $\frac{T_g - T_f}{T_g - T_{c,e}}$
ρ - Density
σ - Stress
ϕ - Cooling Effectiveness Parameter = $\frac{T_g - T_m}{T_g - T_c}$

XI. REFERENCES

1. Stabe, Roy G. and John F. Kline, "Aerodynamic Performance of a Core-Engine Turbine Stator Vane Tested in a Two-Dimensional Cascade of 10 Vanes and in a Single-Vane Tunnel," NASA TMX-2766, 1973.

2. Fish, R.W. and H. McDonald, "Practical Calculations of Transitional Boundary Layers," *Internal Journal of Heat and Mass Transfer,* Vol 16, September 1973, pp 1729-1744.

3. McAdams, W.H., *Heat Transmission,* 3d ed. (New York: McGraw-Hill Book Company, Inc.,) 1954.

4. Hess, W.G. "Advanced Cooled Turbine Airfoil Aerodynamic Investigation," AFAPL-TR-76-113, February 1977.

DISTRIBUTION LIST
FINAL REPORT, CR-159655
CONTRACT NAS3-20587

1.	NASA-Lewis Research Center 21000 Brookpark Road Cleveland, OH 44135		
	Attn: Report Control Office M.S.	5-5	1
	Technology Utilization Office	3-19	1
	Library	60-3	2
	John E. Dilley	500-305	1
	M. J. Hartmann	5-3	1
	H. E. Rohlik	77-2	1
	F. S. Stepka	77-2	1
	H. J. Gladden	77-2	35
	J. S. Clark	500-202	1
	J. E. Rohde	301-4	1
	C. P. Blankenship	105-1	1
	T. J. Moore	105-1	1
2.	NASA Scientific and Technical Information Facility PO Box 8757 Baltimore/Washington International Airport Maryland 21240 Attn: Accessioning Department		30
3.	NASA TL AFAPL/DO Wright Patterson AFB, OH 45433 Attn: E. E. Bailey		1
4.	Airforce Materials Lab Wright Patterson AFB, OH 45433 Attn: Dr. Norman Tallan		1
5.	Arnold Airforce Station Arnold AFS, TN 37389 Attn: Library		1
6.	AiResearch Manufacturing Company 402 South 36th Street PO Box 5217 Phoenix, AZ 85010		
	Attn: Dr. F. B. Wallace		1
	C. E. Corrigan		1
	F. E. Faulkner		1

7. AVCO Corporation
Lycoming Division
550 South Main Street
Stratford, CT 06417
Attn: A. F. DeFerrari — 1

8. Curtiss-Wright Corporation
One Passaic Street
Woodridge, NJ 07075
Attn: Dr. Sam Wolisin — 1

9. Electric Power Research Institute
3412 Hillview Avenue
PO Box 10412
Palto Alto, CA 94303
Attn: Dr. Arthur Cohn — 1

10. General Electric Company
Advanced Product Planning
Schenectady, NY 12301
Attn: Dr. William H. Day — 1

11. General Electric Company
Gas Turbine Products Division
Schenectady, NY 12301
Attn: Dr. J. E. Palko — 1

12. General Electric Company
Flight Propulsion Division
Cincinnati, OH 45215
Attn: M. Zipkin — 1
H. Maclin — 1

13. General Electric Company
1000 Western Avenue
Lynn, MA 01910
Attn: Arne Brook
Mail Drop 240 6B — 1

14. General Motors Corporation
Detroit Diesel Allison
PO Box 894
Indianapolis, IN 36206
Attn: D. A. Nealy — 1
D. Klingman — 1
W. C. Davis — 1

15. International Harvester Corporation
Solar Division
PO Box 80966
San Diego, CA 92138
Attn: Dr. Arthur Metcalfe 1
D. M. Evans 1

16. National Aeronautics and Space Administration
Ames Research Center
Moffett Field, CA 94035
Attn: Library 1

17. National Aeronautics and Space Administration
NASA Headquarters
Washington, D.C. 20546
Attn: G. Banerian M.S. RTP-6 1
L. Harris RTM-6 1
R. Rudey RTP-6 1

18. National Aeronautics and Space Administration
Flight Research Center
PO Box 273
Edwards, CA 93533
Attn: Library 1

19. National Aeronautics and Space Administration
Langley Research Center
Hampton, VA 23665
Attn: Library 1

20. U.S. Energy Research and Development Administration
Division of Conservation Research and Technology
Washington, D.C. 20545
Attn: John Neal 1
Erick Lister 1

21. Chief, Materials Engineering Department
Department 93-03-503-4
AiResearch Manufacturing Company of Arizona
402 South 36th Street
PO Box 5217
Phoenix, AZ 85010 1